Thermomagnetic effects in cadmium arsenide

THERMOMAGNETIC EFFECTS IN CADMIUM ARSENIDE

F.A.P. BLOM

THERMOMAGNETIC EFFECTS
IN
CADMIUM ARSENIDE

PROEFSCHRIFT

TER VERKRIJGING VAN DE GRAAD VAN DOCTOR IN DE TECHNISCHE WETENSCHAPPEN AAN DE TECHNISCHE HOGESCHOOL TE EINDHOVEN OP GEZAG VAN DE RECTOR MAGNIFICUS PROF.Dr.Ir.A.A.Th.M. VAN TRIER, HOOGLERAAR IN DE AFDELING DER ELEKTROTECHNIEK, VOOR EEN COMMISSIE UIT DE SENAAT TE VERDEDIGEN OP VRIJDAG 11 DECEMBER 1970 DES NAMIDDAGS TE 4 UUR

DOOR

FRANSISCUS ANTONIUS PETRUS BLOM

GEBOREN TE HAPS

Offset-Drukkerij Biblo 's-Hertogenbosch

DIT PROEFSCHRIFT IS GOEDGEKEURD DOOR DE PROMOTOR

PROF.Dr. C. ZWIKKER

aan thilly
en de jongens

CONTENTS

INTRODUCTION

When a rectangular bar of a semiconductor or a metal is subjected simultaneously to a temperature gradient $\frac{\partial T}{\partial x}$ and a magnetic field in the z-direction, four thermomagnetic effects may occur. Two types of thermomagnetic effects can be distinguished, viz. transverse and longitudinal, analogously to the distinction between the transverse and longitudinal galvanomagnetic effects (Hall effect and magneto-resistance effect, respectively). The transverse Nernst effect (sometimes called the Nernst-Ettingshausen effect) is the appearance of an electric field in the y-direction. The Righi-Leduc effect ("thermal Hall effect") appears as a temperature gradient in the y-direction. The longitudinal effects, viz. the change of the Seebeck effect and of the thermal conductivity, pass under the names of the longitudinal Nernst effect and the Maggi-Righi-Leduc effect, respectively.

Although these effects were already discovered about a hundred years ago, only in recent years has one observed increased attention to the use of thermomagnetic effects in order to gain information on the band structure and the scattering mechanism of the charge carriers in semiconductors. Some of the thermomagnetic effects are particularly sensitive to the interactions of the charge carriers with the crystal lattice, whereas others can provide information on the band structure independent of the nature of the scattering mechanism.

The material chosen to be subjected to these thermomagnetic measurements, Cd_3As_2, is particularly interesting because of the unusually high electron mobility in the case of a material with a tetragonal crystal structure. The relatively poor knowledge of the basic semiconducting properties of this material might be due to the difficulty of preparing physically perfect samples, and the complexity of the band structure.

This thesis deals with extensive experimental investigations of thermomagnetic phenomena in polycrystalline samples of Cd_3As_2 with different electron concentrations. By far most of the measurements have been carried out at room temperature, only a few samples were considered also at liquid nitrogen temperature. The contents of this thesis will be arranged as follows.

In the first chapter we will review the most interesting properties of this compound reported in the literature as well as the interpretations given by the several authors.

Chapter 2 describes the experimental methods used in the investigations, while attention is also paid to the influence of the specimen geometry and the accuracy of the measurements.

In chapter 3 two treatments of the theory of thermomagnetic effects in degenerate n-type semiconductors with non-parabolic conduction bands (of which Cd_3As_2 is believed to be a representative) are reviewed and discussed.

The experimental results concerning the different thermomagnetic phenomena are presented in chapter 4, and will be interpreted by means of the theories outlined in the preceding chapter. The points of agreement and disagreement between theory and experiment will be examined, from which conclusions will be drawn about the transport mechanism in cadmium arsenide.

In the final chapter the predominant features of the work presented in this thesis are reviewed and discussed.

CHAPTER 1

SOME PROPERTIES OF CADMIUM ARSENIDE

In this chapter a survey is given of the most prominent physico-chemical, electrical and thermal properties of Cd_3As_2 reported in the literature.

1.1. *Physico-chemical properties*

The first systematic investigations of the compounds which can be formed with the elements cadmium and arsenic date from 1905 [1]. From the phase diagram of the system Cd-As it can be seen that the compound Cd_3As_2 has a melting point of 721 °C and that there exists a solid-solid transition at about 578 °C [2]. This allotropic phase transformation, which causes a considerable increase in the volume of the unit cell, is mainly responsible for the difficulty of preparing crackfree single crystalline or polycrystalline samples of this material. Many attempts to avoid this cracking by slowly cooling the melt were unsuccessful [3,4,5]. Even if the material has been annealed at a temperature just below or just above the transition temperature for a period of 2 or 3 days, many of these samples have to be discarded because of cracks [6]. The only procedure to solve this problem seems to be vapour phase growth at low temperatures.

Koltirine and Chaumereuil [7] succeeded in growing small crystals by using a sublimation process: a stream of hydrogen was passed through an open silica tube in which a piece of cadmium arsenide had been placed at about 600 °C. Depending on the temperature gradient along the tube and the velocity of the carrier gas, small single crystals of different habit (cubes, needles, pyramids) condensed at the colder ends of the tube. However, because of their geometry these crystals cannot be used as samples in thermomagnetic measurements.

The same authors reported a modified method of growing much larger single crystals. An evacuated silica ampoule containing polycrystalline cadmium arsenide was placed in a two-zone furnace. By pulling the ampoule very slowly (pulling rate 1 mm/day) through an abrupt temperature step from 560 °C to 550 °C, a crystal of 4 cm length and a diameter of 5 mm was obtained. A similar technique has been applied by Matsunami [8].

X-ray analyses have shown [9] that the unit cell of Cd_3As_2 in the low temperature phase is tetragonal (a = 12.67 Å, c = 25.48 Å) and belongs to the space group $I4_1cd$, in which the As-ions are approximately cubic close-packed. Each As-ion is surrounded by Cd-ions at 6 of the 8 corners of a distorted cube. The unit cell contains 32 formula units, i.e. 64 As-ions and 96 Cd-ions. The structure of the high temperature phase of cadmium arsenide is still unknown [10].

Doping of the material may be achieved by adding the dopants directly to the starting material [6,11]. In general the influence of impurities on the number of free electrons is weak, even up to doping levels of a few per cent. From the literature it appears that it is difficult to prepare samples with electron concentrations much lower or higher than about 2×10^{24} m^{-3}. Up to now samples with p-type conductivity have never been reported.

1.2. *Electrical and thermal transport phenomena*

Since the discovery of Cd_3As_2 as an n-type semiconductor with a high electron mobility [12], about 1 m^2/Vs at room temperature, much work has been done concerning the electrical and thermal transport properties of this II-V-compound. The first interesting feature is the striking similarity between the electrical properties of this compound and those of other high-mobility semiconductors, such as InSb, HgTe and HgSe, although cadmium arsenide does not crystallise in the cubic zincblende structure. Moss [13] established that the material was a photoconductor and reported an electrical and optical band gap of 0.14 eV and 0.60 eV, respectively. The large discrepancies of the values of the band gap [14] quoted in the literature, together with the large magneto-resistance effect [15,16] indicate a complex band structure. Turner et al. [17] estimated the effective

mass of the conduction electrons from the Seebeck coefficient. For a sample of an electron concentration of 3×10^{24} m^{-3} and a Seebeck coefficient of 140 μV/K at room temperature they found an effective mass of 0.10 m_o ($\pm$ 0.05 m_o). The thermal conductivity at room temperature was reported to be 11 W/mK, the highest value ever found for this compound. More extensive studies of the Seebeck effect, the Hall effect and the electrical conductivity as functions of temperature by Sexer as well as Zdanowicz [11,18], led to the following hypotheses

a. the electron gas of Cd_3As_2 is strongly degenerate;
b. there exists a single conduction band with a parabolic dependence of the energy on the magnitude of the wave number of the electrons;
c. the scattering of the conduction electrons is caused by interaction with acoustical lattice vibrations.

The values of the electron effective masses reported in the references 11 and 18 were 0.050 m_o and 0.046 m_o respectively. It should be mentioned that the electron concentrations of the samples used by the two authors were also nearly equal (2×10^{24} m^{-3}).

Later work by Sexer[19] however proved that the value of m^* is dependent on the number of conduction electrons n: in the range from 10^{24} to 10^{25} m^{-3} the effective mass increases about a factor two. The discovery of this phenomenon in cadmium arsenide resulted in the rejection of hypothesis b: for, the effective mass in case a parabolic band applies is constant. Afterwards, two main opinions concerning the conduction band structure were represented in the literature

1. two parabolic conduction bands;
2. a single non-parabolic conduction band, first proposed by Kane for InSb[20].

Sexer was the first representative of the group of authors to suggest a two-band model [16,21]. The energy separation between the lower lying band of $m^* = 0.060$ m_o and the higher lying one of $m^* = 0.120$ m_o was calculated to be 0.15 eV. For the fundamental band gap E_g, in this case the distance between the top of the valence band and the bottom of the light electron band, a value of 0.14 eV was found. Hypothesis a was changed in such a way that the light electrons were always strongly degenerate, whereas the heavy electrons were supposed to obey Maxwell-Boltzmann statistics for not too high concentrations. With Sexer's model and the assumption of acoustical

lattice scattering, a qualitatively good explanation could be given for the dependence of m^* on n and for the magneto-resistance. An alternative explanation of her experimental results, viz. by non-parabolicity of the conduction band, has been rejected by Sexer on account of obscure arguments [21].

Lovett and Ballentyne [5,22] studied thermomagnetic effects on polycrystalline samples of $n = 2 \times 10^{24}$ m^{-3} and found a good agreement between the experiments and the theory for a single parabolic conduction band in combination with acoustical lattice scattering. Some doubt is justified concerning the low temperature value of $m^* = 0.090\ m_o$ and their explanation of the disagreement between theory and experiments at low temperatures. In a sample of high electron concentration the authors found a considerable deviation from this simple theory. This deviating result was explained by using a slight modification [23] of Sexer's two-band model.

Two recent contributions to the two-band model were published in 1969. Shevchenko et al. [24] assert that, if the electrons of both kinds are scattered in the same way (by acoustical phonons) and no other type of scattering occurs, they find a good theoretical fit for the dependence of the Seebeck coefficient on the electron concentration. The parameters they chose were $m_1^* = 0.045\ m_o$, $m_2^* = 0.090\ m_o$ and $E_{12} = 0.12$ eV. Hall effect studies by Lovett [25] on quenched samples also indicate the presence of two types of electrons of highly different mobilities. Suitable room temperature values of carrier concentrations and mobilities in the lower and upper bands were found to be $n_1 = 3 \times 10^{24}$ m^{-3}, $\mu_1 = 1.2$ m^2/Vs, $n_2 = 1 \times 10^{27}$ m^{-3}, $\mu_2 = 0.0055$ m^2/Vs. The author noticed, however, that these values are not unique; increasing μ_2 by a factor 3 and correspondingly decreasing n_2 by 3, still gives reasonable agreement with experimental values. A remarkable point is that some samples prepared by vapour deposition showed no decrease in the Hall coefficient with increasing magnetic field, the effect upon which Lovett's proposal is based.

The first suggestion to explain the variation of m^* with n by applying a non-parabolic conduction band comes from Haidemenakis et al.[26]. From magneto-optical studies on single crystals of $n = 2 \times 10^{24}$ m^{-3} they established that m^* is a slightly varying function of the temperature. Typical values are $0.045\ m_o$ and $0.041\ m_o$ near 300 K and 4 K respectively.

After a heat treatment of these crystals the number of carriers increased by a factor two, and the new effective mass ratios were 0.054 and 0.045 at near room temperature and liquid helium temperature, respectively. The author also found a very slight increase in effective mass with increasing magnetic field. These phenomena, the variation of m^* with electron concentration, temperature and magnetic field, are reminiscent of the case of lead salt semiconductors, implying non-parabolicity of the conduction band. An energy gap of cadmium arsenide equal to $E_g = 0.025$ eV is reported by the authors.

Rosenman[27] observed Shubnikov- de Haas effects in oriented single crystals of Cd_3As_2 and proved that in the range of low concentrations there is only one type of electrons. The Fermi surface consists of only one ellipsoid, which is a revolution ellipsoid about the 4-fold c-axis. The ellipsoid is elongated in the c-direction, which leads to a cyclotron mass of $m^*_{\parallel} = 0.050\ m_o$ for the c-axis parallel to the magnetic induction, and of $m^*_{\perp} = 0.060\ m_o$ for the magnetic induction in the directions perpendicular to the c-axis.

Armitage and Goldsmid[28] derived the concentration dependence of m^* from the saturation magneto-Seebeck and Hall coefficients at 80 K. The results could be interpreted in terms of a Kane-type conduction band. Making the assumptions that m^* can be neglected as compared with m_o and that the band gap is much smaller than the spin-orbit splitting energy, they found a value of P equal to 8.3×10^{-8} eVcm. The parameter P of Kane's equation will be discussed in later chapters. At the same time Rosenman and ourselves confirmed this proposal from measurements of the Shubnikov-de Haas effect at liquid helium temperature [29] and from thermomagnetic measurements at room temperature [30], respectively. Rosenman was not able to calculate the numerical value of P, but he reported a value of 15 ± 2 eV for the quantity Q, a parameter which is closely related to P. We reported room temperature values of both P and Q and also made an estimate of $m^*(0)$, the effective mass at the bottom of the Kane conduction band. Using the values $P = 8.1 \times 10^{-8}$ eVcm, $Q = 12$ eV and $m^*(0) = 0.012\ m_o$ a value of 0.15 eV was obtained for the band gap of Cd_3As_2. Apart from the fact that in the results mentioned above no corrections were made for the finite spin-orbit splitting energy, it is of interest that the values of P reported for cadmium arsenide are so close to those observed for III-V-compounds. This point will be further discussed in chapter 4.

A Kane band model and scattering by acoustical phonons, however, is contradictory to the signs and magnitudes of the thermomagnetic transport coefficients. Therefore, scattering by optical phonons has been adopted by us [30]. Assuming this type of scattering, a reasonably good agreement was obtained between theory and experiments. Such a scattering mechanism could also be responsible for the partly inelastic collisions of the electrons at about 100 K [31,32].

It should not be forgotten that a serious disadvantage of this band model is that it does not explain the large magneto-resistance effect. More attention to this problem will be paid in chapter 5.

The most recent proposal about the band structure of cadmium arsenide by Wagner et al. [33a] is based on the similarity between the interband magneto-absorption spectra of $Cd_xZn_{3-x}As_2$ and $Cd_xHg_{1-x}Te$-systems. This suggests an α-Sn or HgTe band structure, with $P = 9.1 \times 10^{-8}$ eVcm and $E_g = 0.38$ eV. In contrast with the calculations of P and E_g in reference 30, in these calculations a small spin-orbit splitting energy was assumed. Theoretical investigations by Lin-Chung [33b] predict a band structure of Cd_3As_2 in favour of the latter model.

CHAPTER 2

EXPERIMENTAL METHODS

In the first section of this chapter a description will be given of the methods used for preparing polycrystalline samples of cadmium arsenide. After that the experimental set-up used for measuring the transport coefficients will be described. The chapter concludes with remarks on corrections and on the accuracy of the measurements.

2.1. *Preparation of the samples*

The investigated samples were prepared in two steps. First, undoped starting material was obtained by reacting stochiometric quantities of spectrographically pure cadmium† and arsenic§ in a sealed silica ampoule. The inside surface of the ampoule had been carbon-coated by the pyrolysis of petroleum ether to prevent sticking of the material to the wall. The ampoule was heated to about 200°C above the melting point of Cd_3As_2 (721°C) and kept at this temperature for several hours. After this period the furnace was slowly cooled to room temperature without further precautions. The ingot of the ampoule consisted of polycrystalline material, which had many cracks due to the solid-solid transition. Ingots obtained in this way were used as starting material for the second preparation step.

Quartz ampoules (inside dia. 8 mm) were filled with charges of 20 g of this material. When desirable, at this stage small amounts of doping

---

† *Cadmium bars (purity 99.9999 %) were obtained from Koch-Light Lab. Ltd., Colnbrook, England.*

§ *Arsenic lumps (purity 99.9999 %) obtained from Société Générale des Minerais (Hoboken), Bruxelles, Belgique.*

elements (Ge, Ga, Ni, S, Si) were added directly to the material. It should be noted that the ampoules had not been carbon-coated. Experiments have shown that it was not cadmium arsenide but liquid cadmium which was responsible for the contamination of the quartz[34]. Before the ampoule was sealed off a cylindrical bar of high-pure graphite was placed on top of the material. This bar had a twofold purpose. Probably it acted as an absorber of undesirable gases escaping from the material during heating, since the ingots obtained had a perfectly clean, mirror-like surface when graphite was used. Secondly, the bar when floating on the molten Cd_3As_2 suppressed the boiling effect of the liquid. Without the use of such a bar, many macroscopic holes were formed in the ingot; in some experiments even tube-like ingots were obtained. After a period of 6 hours at 900°C the ampoule was quenched to room temperature. Microscopic observations on polished slabs showed that the grains in quenched ingots were considerably smaller than those in slowly cooled ones. The main advantage of the quenching procedure is that the material is perfectly free from cracks. A similar behaviour was observed in quenched samples of $CdSnAs_2$ [35], a material which is also difficult to prepare because of a solid-solid transition. X-ray studies suggested that the material was single phase, and no differences were found between X-ray diffraction patterns of quenched ingots and those of single crystals grown from the vapour phase. So we assume this material to have the low temperature phase; we would observe that attempts to obtain Cd_3As_2 samples in the high temperature phase by quenching have been unsuccessful [10].

The cylindrical ingots were ground and polished to rectangular samples, having dimensions of about 25mm × 5mm × 5mm, and subjected to preliminary measurements to determine the electron concentration and the Hall mobility. In general the electron mobilities of the quenched samples are rather low; therefore, they were subjected to various heat treatments in evacuated silica tubes. This annealing produced variations in electron mobility but not of a very systematic kind, whereas the carrier concentration did not deviate much from the initial value [34]. Despite this non-reproducible annealing process we mostly succeeded in enlarging the electron mobility by a factor 2 or 3. Only samples with acceptable values of the electron mobility (about 1 m^2/Vs) have been used in our experiments.

The influence of impurities on the electron concentration is not very pronounced. Apparently Ag and Au act as acceptors; Si, Ga, Ge and S play

the part of donors, while the behaviour of Cu and Ni in cadmium arsenide seems complicated. There is a strong effect of the impurity elements on the mechanical properties of the samples. By adding Ni and Si and, to a lesser extent also Ge, the samples exhibit a higher mechanical strength and a higher microhardness. Cu-doped and particularly S-doped samples are very brittle and difficult to handle.

2.2. Measuring methods

An apparatus has been designed for measuring the main electrical, thermoelectric, galvano- and thermomagnetic transport coefficients at room temperature and at liquid nitrogen temperature. With this measuring equipment we are able to investigate the electrical conductivity, Hall effect, magneto-resistance, Seebeck effect, Righi-Leduc effect, transverse and longitudinal Nernst effect, thermal conductivity and Maggi-Righi-Leduc effect. The apparatus, shown in Fig.2-1, consists of a cryostat of all-metal construction, whose lower part is placed between the poles of an electromagnet (Newport Type E). With an air gap of 25 mm the magnetic induction can be varied up to 1.5 Wb/m^2. The inner chamber (1) of the cryostat is filled with water or liquid nitrogen. The space between the inner and the outer tube (2) can be evacuated to a pressure of 10^{-5} mm Hg, to ensure "adiabatic" conditions when carrying out thermomagnetic measurements. The sample is mounted in the sample holder (3) which is in good thermal contact with the can that contains the refrigerant. Inside the cryostat the leading-in wires are twisted and locked up in metal tubes (4) in order to diminish pick up from stray fields. From the lead seal to the reference temperature bath (5) each wire is enclosed by a thin copper tube (6). Fig.2-2 shows the details of the sample holder and the way the sample is mounted. On to the bottom of the can which contains the cooling liquid, a rectangular copper frame (7) is soldered. Two copper plates (8) on the front and back of the frame serve as radiation shields, so that the sample is surrounded by a box which is at constant temperature. Both on the left and right hand sides of the frame 6 feed-through seals are provided for the extension leading-in wires (dia. 1 mm). Of the 12 wires (8 of copper, 4 of constantan) 4 pairs of copper and constantan are used as extension wires

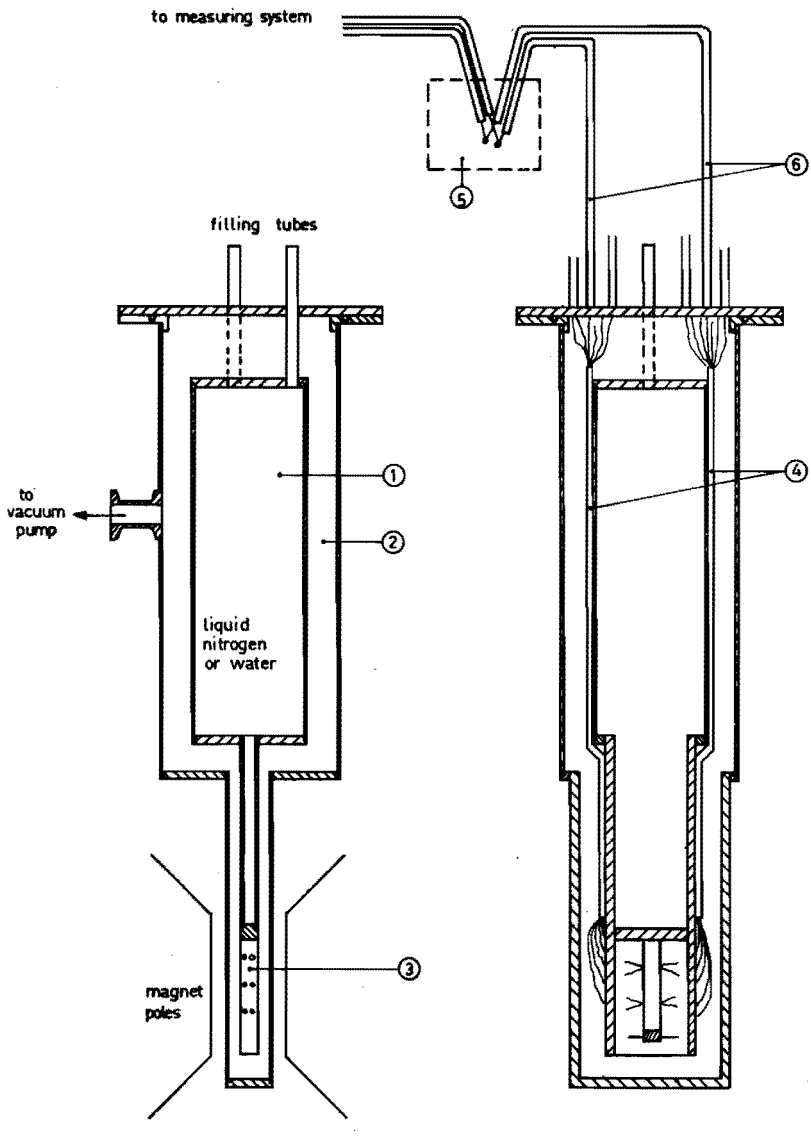

Fig. 2-1 Apparatus for measuring the thermomagnetic effects. For explanation, see text.

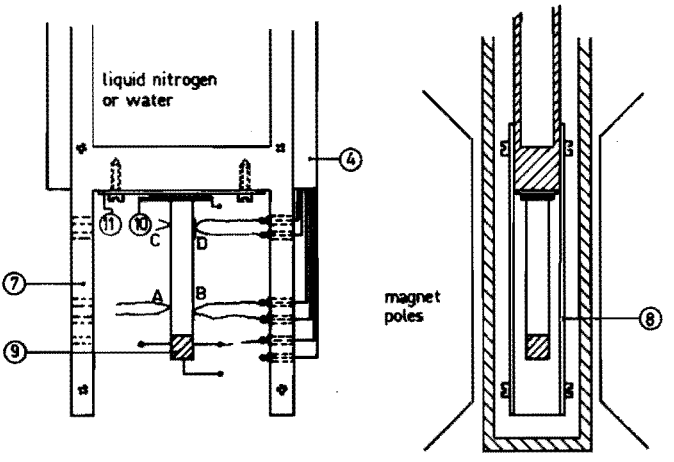

Fig. 2-2 Details of the sample holder assembly.

for the Cu-Con-thermocouples on the sample. The remaining 4 copper wires are needed for the gradient heater (9) : 2 for the current supply and 2 for measuring the voltage across the heater. When performing galvanomagnetic measurements, the latter two are unfastened from the heater and connected to the samples as current leads.

The advantage of the sample holder is that when measuring a number of samples, each sample can be simply replaced by another. On the other hand it has the disadvantage that the thermocouples are not unbroken, which enhances the possibility of spurious thermal e.m.f's developing in the leads. To diminish this inaccuracy the thermocouples are calibrated under the same conditions as during the measurements.

The sample is cemented to a thin copper plate (10) with an electrically conducting adhesive†. The copper plate serves as one of the current contacts for galvanomagnetic measurements. The sample can be screwed on to the heat sink by means of a second copper plate (11), which is electrically insulated

---

† *Eccobond solder 56C, volume resistivity less than* 2.10^{-4} *Ωcm, from Emerson and Cuming, Inc., Canton Massachusetts.*

from the contact plate (10) by a thin layer of Stycast 2850 GT[§]. The surface between the plate (11) and the heat sink has been greased with a liquid alloy solder[§§] to reduce the thermal resistance of the contact. At the other end of the sample a small heater is attached to establish a temperature gradient along the sample. About 100mW-power is sufficient to obtain a temperature gradient of 10^{o}C/cm. The gradient heater consists of Zener diodes with small temperature coefficients. Hence, using a current source, the totally developed quantity of heat remains constant over a wide temperature range. In fact, a particular combination of Zener diodes showed to have a relative variation of the voltage smaller than 1 : 10^4 in the temperature range from 80 to 320 K. It appeared that the voltage was also independent of the applied magnetic field, so no corrections were necessary for the "magneto-resistance" of the heater. These properties give the Zener heater considerable advantages over a conventional wire-wound one. The use of a constant-power heater greatly improves the accuracy of difficult measurements, such as those of the Maggi-Righi-Leduc effect. The diodes are embedded in an epoxy resin (Stycast 2850 GT) and as a whole enclosed in a small copper box. This cover is electrically connected to the sample and can be used as the other current contact.

The longitudinal and transverse voltages and temperature differences are measured by four Cu-Con-thermocouples (A, B, C and D). Three of the couples are soldered to the sample with Sn-solder, while the fourth is mostly electrically insulated from the sample by a thin layer of Stycast. With the thermocouples A, B and C all desired effects can be observed; whereas, couple D makes it possible to use the thermocouples differentially. The diameter of the Cu and Con-leads is only 50 μm. The location of the contacts on the sample, is such that A and B (C and D) lie opposite each other as accurately as possible, and that A and C (B and D) are placed symmetrically with respect to the ends of the sample.

---

§ *A loaded epoxy resin with a high value of the thermal conductivity (1.8 W/mK) and a very high specific resistivity (about 10^{15} Ωcm); Emerson and Cuming, Inc.*

§§ *Viking-LS 232, Victor King Materials Lab., Palo Alto, California.*

The voltages are measured on a Dieselhorst compensator (Bleeker) or a Keithly 149 d.c. Microvolt-Ammeter. Although the accuracy of the Dieselhorst compensator is much greater than that of the d.c. microvolt meter, the latter has the advantage that the zero suppression up to 100 times full scale of this instrument can be used conveniently for compensating zero-field effects. To ensure stationary heat flow through the sample, the measurements are made 15-30 minutes after the magnetic field has been adjusted. Measurements of the voltages and temperature gradients are made for two opposing directions of the magnetic field. If the results are averaged, errors in the longitudinal and transverse effects due to asymmetrical placing of the contacts cancel out (section 2.3.2, a.1 and b.2).

2.3. Corrections and accuracy

2.3.1. Adiabatic and isothermal transport coefficients

The apparatus has been constructed to reduce to a minimum the heat flow in the directions perpendicular to the main heat flow. This means that we obtain the so called "adiabatic" transport coefficients, whereas for the interpretation of the results the isothermal coefficients are required. The isothermal coefficients for a rectangular sample are calculated from the adiabatic ones by means of the relations

$$\alpha^i = \frac{\alpha^a + N^a B.SB}{1 + S^2B^2} \tag{2.1}$$

$$N^iB = \frac{N^aB - \alpha^a.SB}{1 + S^2B^2} \tag{2.2}$$

$$\kappa^i = \frac{\kappa^i}{1 + S^2B^2} \tag{2.3}$$

where α is the Seebeck coefficient, κ the thermal conductivity, N the transverse Nernst coefficient, S the Righi-Leduc coefficient and B the magnetic induction. The superscripts i and a refer to the isothermal and

adiabatic coefficients, respectively. This confusing nomenclature is due to the two different ways of measuring the thermomagnetic effects. With an electric or a thermal current flowing in the x-direction of a rectangular specimen, the effects can be measured under the conditions that there are no thermal gradients in the y- and z-direction, or that the heat flow in these two transverse directions is zero. The above relations have been derived from the phenomenological equations given in chapter 3. For the definitions of the various isothermal coefficients the reader is also referred to chapter 3. Figs. 2-3 and 2-4 show for a typical sample the differences between the adiabatic and isothermal transverse Nernst and Maggi-Righi-Leduc coefficients.

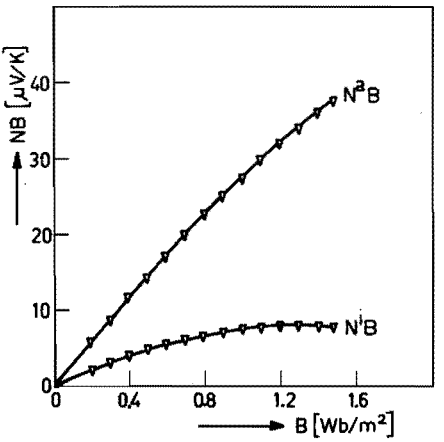

Fig. 2-3

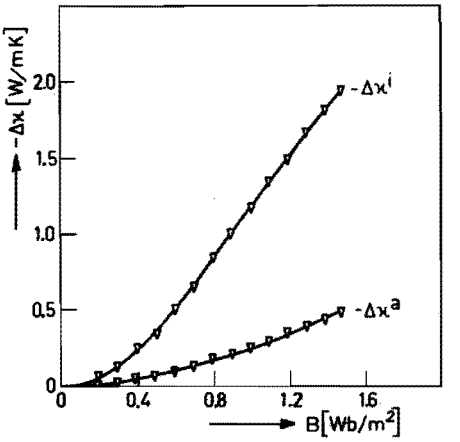

Fig. 2-4

Fig. 2-3 Adiabatic and isothermal transverse Nernst coefficients (sample VII).

Fig. 2-4 Adiabatic and isothermal Maggi-Righi-Leduc coefficients (sample VII).

2.3.2. Influence of the geometry of the sample

The transport coefficients are defined in terms of a specimen of infinite extent, whereas in our experiments rectangular samples of finite dimensions are used. So, in some cases corrections have to be made for the sample geometry in order to compare the experimental results with the definitions. Let us consider Fig.2-5, which gives schematically the location of the thermocouples and the current electrodes on a homogeneous sample. We will examine the geometrical effects on the basis of the transverse and longitudinal galvanomagnetic effects (Hall and magneto-resistance effect); it can be easily proved that the same considerations are valid for the transverse and longitudinal thermomagnetic effects. When using large area current contacts at the ends of the sample the following geometrical effects have to be taken into account.

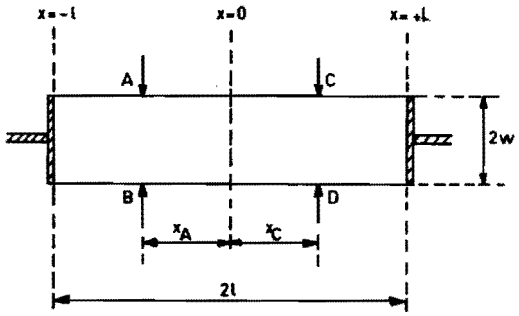

Fig.2-5 Rectangular specimen with large-area current contacts at each end and the locations of the thermocouples.

a. The Hall effect

a.1. First, misalignment of the probes A and B (or C and D) causes an ohmic voltage drop superimposed upon the Hall voltage. Fortunately, this additional voltage cancels out by averaging the voltages measured for two opposing directions of the magnetic field. Nevertheless it is advisable to place the contacts as accurately as possible opposite each other, since for samples

with high electron concentration the ohmic voltage difference can easily be as large as the true Hall voltage, which increases the inaccuracy of the final result.

a.2. Another geometrical effect is the shorting effect[36,37], which appears in samples with large-area current contacts at the ends. The existence of the shorting effect means that the observed coefficient is always smaller than the true Hall coefficient. Isenberg et al.[36] reported numerical results for the ratio $f_H = V_{H,obs.} / V_{H,true}$ in the case that the probes are placed exactly in the middle of the sample. The ratio f_H is virtually equal to 1 for a width-to-length ratio $\frac{w}{l}$ of a sample smaller than $\frac{1}{4}$. In our experiments this ratio, however, is not always so small that correction may be negelected. Moreover, as can be seen in Fig.2-5, the Hall probes are not placed in the middle of the sample.

With the help of the solution of the Laplace equation under simplified conditions, as given by Volger[37], we have calculated numerically the form factor f_H as a function of $\frac{x}{l}$ for different values of $\frac{w}{l}$. These calculations are valid for ideal current contact material and no allowance is made for the fact that f_H also depends on the Hall angle[38]. Some of our results are shown in Fig.2-6. We also determined experimentally the ratio f_H for different values of $\frac{x}{l}$ and $\frac{w}{l}$ on a "centipede" of bismuth. As can be seen from the figure the agreement with theory is rather good. The horizontal bars through the experimental points indicate the widths of the contact probes relative to the length of the specimen.

The measured values of the Hall, transverse Nernst and Righi-Leduc coefficients have been corrected with the form factor f_H to obtain the true values of the three coefficients.

b. The magneto-resistance effect

b.1. It has been shown[38,39] that the shorting effect also produces an increase in the magneto-resistance effect measured on a sample with finite dimensions. The measured magneto-resistance is

$$\frac{\rho_m(B)}{\rho_o} = (1 + \frac{\Delta\rho}{\rho_o})\ (1 + f_R) \qquad (2.4)$$

where $\frac{\Delta\rho}{\rho_o}$ is the true magnetoresistance of an infinitely long sample, ρ_o is the resistivity in the absence of a magnetic field, and f_R denotes the relative effect due to shorting. The quantity f_R depends on the width-to-length ratio $\frac{w}{l}$, the relative distance between the probes and the end contacts $\frac{l-x}{l}$, and the Hall angle θ.

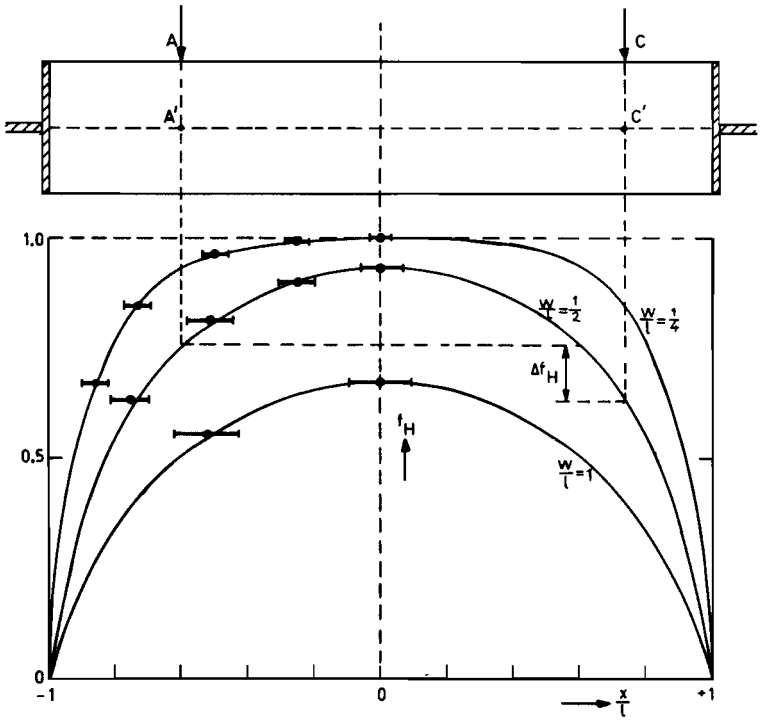

Fig. 2-6 *Form factor f_H in eq. (2.5) as a function of $\frac{x}{l}$, for different ratios of $\frac{w}{l}$, which also illustrates the error in the longitudinal effect due to misalignment.*
The points are experimental results found on a "centipede" of bismuth.

Numerical calculations by Drabble and Wolfe[39] show that when the probes are placed at a distance from the end equal to or greater than the width of a specimen with $\frac{w}{l} \leq \frac{1}{2}$, f_R is always smaller than 10^{-3}, even up to values of μB (tan θ) greater than 10. Comparing this systematic error in the longitudinal effects (magneto-resistance, longitudinal Nernst, and Maggi-Righi-Leduc effect) with other errors, we conclude that in our cases this correction is always negligible.

b.2. A second interesting geometrical effect on the magneto-resistance (and the other longitudinal effects) can be illustrated with the help of Fig.2-6. If the longitudinal probes are placed assymetrically on the sample ($x_A \neq x_C$), the voltage measured between A and C consists of two contributions :

$$V_m(B) = V_o \left(1 + \frac{\Delta\rho}{\rho_o}\right) (1 + f_R) \pm \frac{1}{2} V_o \mu B \frac{w}{l} \{f_H(A) - f_H(C)\} \qquad (2.5)$$

The first term in the right hand side of this relation arises from the true magneto-resistance corrected for the geometry effect (see eq.(2.4)). The second term is caused by the assymetrical placing of A and C; in fact it is the difference between the two Hall voltages which would be measured between the points A and A', and C and C', respectively. It should be noted that in samples with high mobility and with badly chosen geometry, the magnitude of the second term may greatly exceed that of the first. Fortunately, as has been remarked before, the second term is linear in B and therefore cancels out by averaging the measurements for two opposing directions of B.

2.3.3 General remarks on the accuracy of the measurements

As is well known, accurate measurements of the thermal conductivity are difficult, which is evidenced by frequent disagreement found between the results for the same material by different workers. This conclusion is the more justified in the case of measurements of thermomagnetic effects. The measuring method described in section 2.2 is a steady-state technique, in which it is required that the quantity of heat developed by the heat source

should be equal to the quantity of heat transferred to the heat sink. This means that the transverse heat losses from the sample and the heater to the surrounding parts of the apparatus must be kept to a minimum. The main sources of error are due to radiation loss from the sample and to conduction of heat by the thermocouples and the lead wires of the heater. In order to minimise the error due to convection, the sample holder assembly is kept in a high vacuum (10^{-5} mm Hg). Since radiation loss is proportional to the fourth power of the absolute temperature, this source of error may be neglected at room temperature. Nevertheless, a radiation shield in good thermal contact with the heat sink has been provided, so that also at liquid nitrogen temperature the temperature differences between the sample and the surrounding shield are small. The heat conducted by the thermocouples and the lead wires require serious attention. Twelve wires are needed for the measurements, of which four are of copper with very high thermal conductivity. However, most of the conventionally used pairs of thermocouples, except Cu-Con, exhibit a magnetic field dependent thermal e.m.f. So we tried to find the solution for this problem by minimising the cross-sectional areas of the copper and constantan wires. Most of the measurements have been carried out using Cu and Con-wires of 50 μm in diameter, while in some experiments Cu-wires with a diameter of only 25 μm have been used. Estimates of the heat losses due to radiation and thermal conduction in the leads, based on the theoretical and experimental results relating to the errors in a Harman apparatus[40], indicate that this error can be kept within about 1% at room temperature as well as at liquid nitrogen temperature.

It is believed that the electrical measurements of the quantity of heat, the longitudinal and transverse voltages and thermal e.m.f.'s can be carried out with an accuracy better than 0,5 %, so that these errors may be neglected with respect to others. The differences between the thermal e.m.f.'s of the various Cu-Con-couples are also found to be negligible.

The magnetic field has been calibrated by a magnetometer with an accuracy of 0.1% (Newport type J).

The main source of errors in the results concerning the adiabatic coefficients lies in the inaccuracy of the distances between the thermocouples on the sample. The dimensions of the sample in the y-direction (distance AB in Fig. 5) and z-direction (the width of the sample in the direction of the magnetic field) can be measured with an accuracy of 1 - 2%. However, the

distance AC (or BD) can hardly be obtained within 5%, also because of the relatively large contact areas. Apart from the Seebeck coefficient α^a which is independent of the sample geometry, the accuracy of the other coefficients κ^a, SB and N^aB is mainly determined by the accuracy of the distances between the longitudinal probes. The isothermal coefficients which have to be used for comparison with theory and for the calculation of important physical properties, such as the effective mass, electron mobility and electronic thermal conductivity, are determined from the adiabatic ones by eqs. (2.1), (2.2) and (2.3). This conversion increases the inaccuracy in the final results; this is particularly true of the values of the isothermal Nernst coefficient because of the fact that the magnitudes of the quantities N^aB and α^aSB are nearly equal.

Summarising the errors in the measurements of ρ^i, κ^i and SB are believed to be within 6%, an accuracy which is almost entirely determined by the accuracy with which the length AC may be measured. The value of R_H^i, the Hall coefficient, can be obtained with greater accuracy; we estimate the accuracy to be about 4%. As has been mentioned before, the Nernst coefficient has been calculated as the difference between two large quantities which are nearly equal. In general, this leads to an accuracy of only 15 - 20%. The coefficient which may be obtained most accurately is the Seebeck coefficient, since α^i is all but independent of the sample geometry. An additional error arises from the fact that the Seebeck coefficient is measured relative to copper. Corrections for the Seebeck coefficient of copper to obtain the absolute Seebeck coefficient of Cd_3As_2 give some problems, because the history of the copper wire is not always known. Nevertheless the accuracy of α^i is about 3%.

CHAPTER 3

THEORY OF THE THERMOMAGNETIC EFFECTS IN DEGENERATE SEMICONDUCTORS WITH NON-PARABOLIC BAND SHAPES

In this chapter we discuss the various thermomagnetic effects that occur in degenerate semiconductors and the information that these effects provide about the conduction band structure and the electron scattering mechanism. Harman and Honig[41,42] have given an extension to the theory of galvano- and thermomagnetic effects to semiconductors with non-parabolic band shapes (Kane model). Besides this theory, there is another systematic way of describing thermomagnetic phenomena, pioneered by the Polish school of scientists[43], which method is particularly useful in studying the effects of general non-parabolicity on the transport coefficients of degenerate semiconductors. The main results of these two methods will be reviewed, although the treatments cannot always be separated rigorously from each other. Attention will also be paid to the influence of inelastic scattering of the electrons on the transport coefficients.

3.1. Harman's theory[41]

This theory is applicable when the following conditions are fulfilled:

- a single conduction band with constant energy surfaces of spherical symmetry;
- a not necessarily quadratic dependence of the electron energy on the magnitude of the wave vector;
- an arbitrary magnetic field below the quantum region;
- the existence of a relaxation time which is a function of the electron energy.

For electrons in a solid which are subjected to externally applied forces due to temperature gradients, electric and magnetic fields, the Boltzmann transport equation reads[45]

$$-\frac{e}{\hbar}\left(\vec{\nabla}_{\vec{k}}\frac{E_B}{e}+\vec{v}\times\vec{B}\right).\vec{\nabla}_{\vec{k}}f+\vec{v}.\vec{\nabla}_{\vec{r}}f=-\frac{f-f_o}{\tau} \qquad (3.1)$$

where e is the absolute value of the electron charge, $\vec{v}$ is the group velocity $\vec{v}=\frac{1}{\hbar}\vec{\nabla}_{\vec{k}}\varepsilon$, f is the perturbed distribution function, f_o the Fermi-Dirac distribution function, τ the relaxation time, $\vec{B}$ the magnetic induction, $\vec{\nabla}_{\vec{r}}$ and $\vec{\nabla}_{\vec{k}}$ are the nabla operators in $\vec{r}$- and $\vec{k}$-space, and $\vec{\nabla}_{\vec{r}}E_B$ is the gradient of the band edge with position in real space. The energy of an electron can be written as $E = E_B(x) + \varepsilon(k)$, where $\varepsilon(k)$ is the kinetic energy relative to the appropiate band edge and x is a generalized position coordinate (see Fig.3-1).

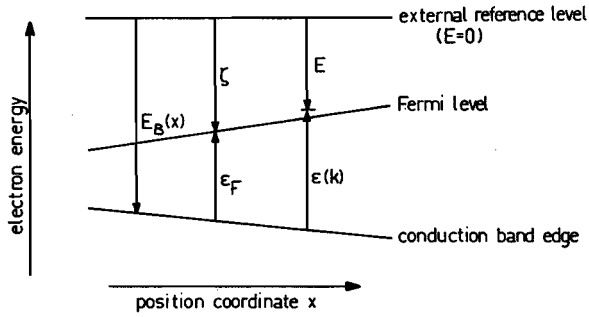

Fig. 3-1 Schematic diagram illustrating the interrelations between E, E_B, ε_F, ε *and* ζ. *Note that* ε_F *and* $\varepsilon(k)$ *are taken as positive, whereas* E, E_B *and* ζ *are negative, so that* $E = E_B(x) + \varepsilon(k)$ *and* $\zeta = E_B(x) + \varepsilon_F$.

Introducing the quantity

$$\vec{F}=-e\,\vec{\nabla}_{\vec{r}}\frac{E_B}{e}-T\,\vec{\nabla}_{\vec{r}}\frac{\varepsilon_F}{T}-\frac{\varepsilon}{T}\vec{\nabla}_{\vec{r}}T \qquad (3.2)$$

where ε_F is the Fermi level relative to the band edge E_B, and assuming that

$$f = f_o - \vec{v} \cdot \vec{\Psi} \frac{\partial f_o}{\partial \varepsilon} \tag{3.3}$$

it can be verified that for spherically symmetric $\varepsilon(k)$, eq. (3.1) reduces to

$$\left[\vec{F} + \frac{e}{m^*} (\vec{B} \times \vec{\Psi}) - \frac{\vec{\Psi}}{\tau} \right] \cdot \vec{v} = 0 \tag{3.4}$$

In equation (3.4), m^* is the momentum effective mass defined by

$$m^* = \frac{\hbar^2 k}{\frac{d\varepsilon}{dk}} \tag{3.5}$$

It has been proved[41,44] that the effective mass which enters the Boltzmann equation in the formulation presented here, is the quantity (3.5). Only for bands of standard form, for which $\varepsilon = \hbar^2 k^2 / 2m^*$, the quantity (3.5) does become equivalent to the commonly cited relation

$$m^{**} = \frac{\hbar^2}{d^2\varepsilon / dk^2} \tag{3.6}$$

For the case of a transverse magnetic field for which $\vec{B}$ is perpendicular to $\vec{F}$, and $\vec{B}$ lies along the z-axis of a rectangular coordinate system, it can be shown that the solutions of eq. (3.4) for Ψ_x and Ψ_y are

$$\Psi_{x,y} = (\tau F_{x,y} \mp \omega\tau^2 F_{y,x}) / (1 + \omega^2\tau^2) \tag{3.7}$$

where ω is defined as $\omega = - e B_z / m^*$, the cyclotron resonance frequency. In order to obtain a set of phenomenological equations, let us consider the transport of electric charge and of kinetic energy ε due to the motion of electrons

$$\vec{J} = -\frac{e}{4\pi^3}\int \vec{v}\, f d^3\vec{k} = \frac{e}{\pi^2}\int \vec{v}\,(\vec{v}.\vec{\Psi})\,\frac{\partial f_o}{\partial \varepsilon}\, k^2\, dk \tag{3.8}$$

$$\vec{W} = \frac{1}{4\pi^3}\int \varepsilon\vec{v}\, f d^3\vec{k} = -\frac{1}{\pi^2}\int \varepsilon\vec{v}\,(\vec{v}.\vec{\Psi})\,\frac{\partial f_o}{\partial \varepsilon}\, k^2\, dk \tag{3.9}$$

Using eqs. (3.8) and (3.9) together with eq. (3.7) and assuming that the material is homogeneous†, one arrives at the following set of equations (3.10) for a rectangular parallelepiped geometry

$$\begin{bmatrix} J_x \\ J_y \\ W_x \\ W_y \end{bmatrix} = \begin{bmatrix} e^2K_1 & -e^3G_1B_z & -\frac{e}{T}(K_1\varepsilon_F - K_2) & \frac{e^2B_z}{T}(G_1\varepsilon_F - G_2) \\ e^3G_1B_z & e^2K_1 & -\frac{eB_z}{T}(G_1\varepsilon_F - G_2) & -\frac{e}{T}(K_1\varepsilon_F - K_2) \\ -eK_2 & e^2G_2B_z & \frac{1}{T}(K_2\varepsilon_F - K_3) & -\frac{eB_z}{T}(G_2\varepsilon_F - G_3) \\ -e\,G_2B_z & -eK_2 & \frac{eB_z}{T}(G_2\varepsilon_F - G_3) & \frac{1}{T}(K_2\varepsilon_F - K_3) \end{bmatrix} \times \begin{bmatrix} \nabla_x \frac{\zeta}{e} \\ \nabla_y \frac{\zeta}{e} \\ \nabla_x T \\ \nabla_y T \end{bmatrix}$$

in which the Onsager-Casimir reciprocity relations among the coefficients of $\nabla \frac{\zeta}{e}$ and ∇T are satisfied. The various macroscopic coefficients are given by

$$K_i = -\frac{4}{3h^2}\int_0^\infty \frac{\varepsilon^{i-1}\tau k^2 (d\varepsilon/dk)(\partial f_o/\partial\varepsilon)d\varepsilon}{1 + \omega^2\tau^2} \tag{3.11}$$

$$G_j = -\frac{4}{3h^2\hbar^2}\int_0^\infty \frac{\varepsilon^{j-1}\tau^2 k (d\varepsilon/dk)\,(\partial f_o/\partial\varepsilon)d\varepsilon}{1 + \omega^2\tau^2} \tag{3.12}$$

---

† *Homogeneous material means that the Fermi energy is only dependent on the position coordinates via its temperature dependence :*

$\vec{\nabla}_{\vec{r}}\varepsilon_F = \frac{\partial \varepsilon_F}{\partial T}\vec{\nabla}_{\vec{r}}T.$

and $\zeta = E_B + \varepsilon_F$ is the Fermi-level (or electrochemical potential) relative to the zero energy level (see Fig.3-1). The zero level is defined as the energy of an electron at rest at infinity.

We are now able to set up expressions for the galvano- and thermomagnetic coefficients in terms of K_i and G_j. To this end, we have first to define the various isothermal transport coefficients.
The isothermal electrical conductivity in a magnetic field is defined as

$$\sigma^i(B_z) = (J_x/\nabla_x \tfrac{\zeta}{e}) \text{ with } \nabla_x T = \nabla_y T = J_y = 0 \tag{3.13}$$

The isothermal Hall coefficient is

$$R_H^i(B_z) = (\nabla_y \tfrac{\zeta}{e} / J_x B_z) \text{ with } \nabla_x T = \nabla_y T = J_y = 0 \tag{3.14}$$

The isothermal thermal conductivity in a magnetic field is

$$\kappa^i(B_z) = (-W_x/\nabla_x T) \text{ with } J_x = J_y = \nabla_y T = 0 \tag{3.15}$$

The isothermal Seebeck coefficient in a magnetic field is

$$\alpha^i(B_z) = (\nabla_x \tfrac{\zeta}{e} / \nabla_x T) \text{ with } J_x = J_y = \nabla_y T = 0 \tag{3.16}$$

The transverse Nernst coefficient is

$$N^i(B_z) = (\nabla_y \tfrac{\zeta}{e} / B_z \nabla_x T) \text{ with } J_x = J_y = \nabla_y T = 0 \tag{3.17}$$

Finally it should be noted that the Righi-Leduc coefficient defined as

$$S(B_z) = (\nabla_y T/\nabla_x T) \text{ with } J_x = J_y = W_y = 0 \tag{3.18}$$

is an adiabatic coefficient.

For further calculations it is convenient to use the dimensionless quantities $x = \varepsilon/k_oT$ and $\eta = \varepsilon_F/k_oT$.
If we make use of a general functional relation for the relaxation time of the form[41,44,46]

$$\tau = \tau_o (k^2)^{r-1} \, d\varepsilon/dk \tag{3.19}$$

where r is the scattering parameter, and τ_o is a constant, and also introduce the quantities

$$\beta = \frac{-e \, B_z \, \tau_o \, (k_oT)^2}{\hbar^2} \quad \text{and} \quad g = \frac{4 \, e^2 (k_oT)^2 \, \tau_o}{3h^2}$$

then we may write

$$K_i = (k_oT)^{i-1} \frac{g}{e^2} I_i \tag{3.20}$$

$$G_j = - (k_oT)^{j-1} \frac{g}{e^2} \frac{\beta}{eB_z} J_j$$

where

$$I_i (\eta, r, \beta) = \int_o^\infty \frac{x^{i-1} \, k^{2r} \, (dx/dk)^2 \exp (x-\eta) \, dx}{\{1 + \exp (x-\eta)\}^2 \left(1 + \beta^2 (k^2)^{2r-3} (dx/dk)^4\right)} \tag{3.22}$$

$$J_j (\eta, r, \beta) = \int_o^\infty \frac{x^{j-1} \, k^{4r-3} \, (dx/dk)^4 \exp (x-\eta) dx}{\{1 + \exp (x-\eta)\}^2 \left(1 + \beta^2 (k^2)^{2r-3} (dx/dk)^4\right)} \tag{3.23}$$

With the phenomenological eqs. (3.10), the definitions (3.13) to (3.18), and eqs. (3.20) to (3.23), we obtain

$$\sigma^i (B_z) = \frac{g(I_1^2 + \beta^2 J_1^2)}{I_1} \tag{3.24}$$

$$R^i_H(B_z) = \frac{\beta J_1 / g\, B_z}{I_1^2 + \beta^2 J_1^2} \tag{3.25}$$

$$\kappa^i(B_z) = \kappa_L + \frac{k_o T}{e^2}\, g\left(\frac{I_3 I_1^2 - I_1 I_2^2 + \beta^2 (J_1^2 I_3 - 2 J_1 J_2 J_3 + I_1 J_2^2)}{I_1^2 + \beta^2 J_1^2}\right) \tag{3.26}$$

$$\alpha^i(B_z) = -\frac{k_o}{e}\left(\frac{I_1 I_2 + \beta^2 J_1 J_2}{I_1^2 + \beta^2 J_1^2} - \eta\right) \tag{3.27}$$

$$N^i(B_z) = -\frac{k_o \beta}{e B_z}\left(\frac{J_1 I_2 - J_2 I_1}{I_1^2 + \beta^2 J_1^2}\right) \tag{3.28}$$

If for a band with spherically symmetric energy surfaces the function $\varepsilon(k)$ is known, and if further the dependence of τ on k (the magnitude of r) is substituted in eqs. (3.22) and (3.23), the above relations may be used to calculate numerically the transport coefficients for different values of the reduced Fermi energy and the quantity β. However, both β and g contain τ_o, a constant which can only be obtained in some particular cases, so that the forms of eqs. (3.24) to (3.28) are not adequate to be used for comparison of theory and experiment. Therefore, g and β are expressed in terms of the measurable quantities n and μ (conductivity mobility), via the relation

$$\sigma(0) = n\, e\, \mu = g\, I_1 \quad (\beta = 0)$$

Thus we obtain $g = \frac{n\, e\, \mu}{I_1(\beta=0)}$ and $\beta = -\frac{3\pi^2 n \mu B}{I_1(\beta=0)}$.

3.2. Application of Harman's theory to an n-type semiconductor obeying Kane's band model[42]

In order to explain the experimental results found for InSb, such as the very small electron effective mass and energy gap, Kane[20] calculated the band structure of this compound, assuming that the conduction and valence band extrema are at $k = 0$. A highly non-parabolic conduction band was found :

$$\varepsilon = \frac{\hbar^2 k^2}{2 m_o} - \frac{|E_g|}{2} + \frac{1}{2} \left(E_g^{\,2} + \frac{8}{3} P^2 k^2\right)^{\frac{1}{2}} \tag{3.29}$$

in which P is a matrix element which describes the interaction between the light electron and split-off valence bands. This model is applicable if the spin-orbit splitting energy of the valence band Δ_{so} is much greater than the band gap and kP: $\Delta_{so} >> kP, E_g$. The applicability of the Kane model to III-V-compounds and to certain II-VI-compounds has been amply demonstrated, and it appears that the parameter P has a constant value of about 8.5×10^{-8} eVcm for the materials investigated so far. It appears further that because of the fact that for these semiconductors $m^* << m_o$, the term $\hbar^2 k^2 / 2m_o$ can generally be neglected, so that

$$\varepsilon \simeq -\frac{|E_g|}{2} + \frac{1}{2} \left(E_g^{\,2} + \frac{8}{3} P k^2\right)^{1/2}$$

Introducing the reduced energy gap $x_g = \frac{E_g}{k_o T}$ we find

$$\frac{dx}{dk} = \frac{\sqrt{(4x/\gamma_p)\ (x + x_g)}}{2x + x_g} \tag{3.30}$$

where $\gamma_p = \frac{3}{2} (k_o T/P)^2$

It can be proved that the electron density may be written as

$$n = \frac{1}{2\pi^2} \gamma_P^{3/2} N_1(\eta, x_g) \tag{3.31}$$

where

$$N_1(\eta, x_g) = \int_0^\infty \frac{\sqrt{x(x + x_g)}\ (2x + x_g)}{1 + \exp(x - \eta)}\, dx \tag{3.32}$$

The quantities β and g become

$$\beta = -\frac{3}{8} \mu B_z \gamma_P^{5/2-r} \frac{N_1(\eta, x_g)}{I_1(\eta, x_g, r, 0)}$$

$$g = \frac{\sigma(0)}{4\gamma_P^{r-1} I_1(\eta, x_g, r, 0)}$$

where $I_1(\eta, x_g, r, 0)$ is a special form of the general integral $I_1(\eta, x_g, r, \beta)$ for the case in which the magnetic field is absent.
Using the above results, the integrals presented in eqs. (3.22) and (3.23) may be rewritten for a Kane band as

$$I_i(\eta, x_g, r, \beta) = 4\gamma_P^{r-1} \int_0^\infty \frac{x^{r+1}\ (x+x_g)^{r+1} \exp(x-\eta)\ dx}{(2x+x_g)^2 \left(1+\exp(x-\eta)\right)^2 \{1+\beta^2 \left[x(x+x_g)\right]^{2r-1}/(2x+x_g)^4\}} \tag{3.33}$$

$$J_j(\eta, x_g, r, \beta) = 16\gamma_P^{2r-\frac{7}{2}} \int_0^\infty \frac{x^{2r+j-\frac{1}{2}} (x+x_g)^{2r+\frac{1}{2}} \exp(x-\eta)dx}{(2x+x_g)^4 \left(1+\exp(x-\eta)\right)^2 \{1+\beta^2 \left[x(x+x_g)\right]^{2r-1}/(2x+x_g)^4\}} \tag{3.34}$$

The transport integrals may be evaluated numerically on a computer for different values of the parameters η, x_g, r, P and B_z, and subsequently the corresponding transport coefficients according to eqs. (3.24) to (3.28). Using random values for the various parameters, however, would result in a tremendously large number of curves, from which it would be hardly possible to make comparisons with the experimental results. It is necessary to delimitate the magnitudes of the various parameters in cadmium arsenide. The scattering parameter r gives no trouble : r equals 0, 1, $\frac{1}{2}$ and 2 for scattering by acoustical phonons, optical phonons, neutral and ionized impurities, respectively. Restricting ourselves to room temperature, it is sufficient to vary μB from 0.1 to 2, taking into account a Hall mobility of about 1 m^2/Vs and a maximum attainable magnetic induction of 1.5 Wb/m^2.

A justifiable choice of the magnitude of the reduced Fermi energy is rather difficult, as η is dependent on the band properties E_g and P, which are also unknown beforehand. To solve this problem we proceed as follows. If the conduction band of cadmium arsenide obeys Kane's band model, the quantity $\left(\frac{m^*/m_o}{1-m^*/m_o}\right)^2$ plotted vs. $n^{2/3}$ should be a straight line. From eq. (3.29) it can be found that

$$\left[\frac{m^*/m_o}{1-m^*/m_o}\right]^2 = \frac{9\,\hbar^4 E_g^{\,2}}{16\,m_o^{\,2}P^4} + \frac{3\,\hbar^4(3\pi^2)^{2/3}}{2\,m_o^2\,P^2}\,n^{2/3} =$$

$$= 0.838 \times 10^{-76}\,\frac{E_g^{\,2}}{P^4} + 21.40\quad 10^{-76}\,\frac{n^{2/3}}{P^2} \qquad (3.35)$$

As we will see in the following section, it is possible for degenerate semiconductors to obtain m^* as a function of n from measurements of $\alpha^i(\infty)$ and R_H^i, independent of the scattering mechanism. This means that if the plot of $\left(\frac{m^*}{1-m^*}\right)^2$ vs $n^{2/3}$ gives a straight line, the Kane model is applicable and the slope and the intercept yield values for the band parameters P and E_g. These values can be used to calculate the relationship between n and η from eq. (3.31). For every sample of known electron density n we are now able to determine the reduced Fermi energy.

Assuming a Kane band model with $E_g = 0.15$ and $P = 8.1 \times 10^{-8}$ eVcm we calculated $\frac{\Delta\alpha^i}{\alpha(0)}$, $\frac{\Delta\kappa^i}{\kappa_B(0)}$, $\frac{\Delta\rho^i}{\rho(0)}$, N^i_B and SB as functions of μB in the range of 0 to 2 for two different scattering mechanisms (r=0, 1) and reduced Fermi levels from 4 to 20. A number of these theoretical graphs are presented in the figures of chapter 4 for comparison with experimental results.

3.3. Theory of the Polish school

Harman's theory is particularly useful to calculate the transport coefficients as functions of the magnetic induction for various values of the band and scattering parameters. Confrontation of the experimental data with the various theoretical predictions provide information about the electron scattering mechanism and the degree of non-parabolicity of the conduction band. However, it appears to be difficult to obtain accurate numerical results for the parameters r, E_g and P. For this purpose the theory developed by Kolodziejczak et al.[43] is a more powerful tool, particularly in the case of strongly degenerate semiconductors or semimetals. The main differences between this treatment and the theory of Harman arise from the elimination of the derivative $d\varepsilon/dk$ and the relaxation time τ in the transport integrals K_i and G_j. Using the definition (3.5) for the momentum effective mass and introducing the unaveraged mobility u by $u = e\tau/m^*$, eqs. (3.11) and (3.12) become

$$K_i = \frac{1}{3\pi^2 e} \int_0^\infty \frac{\varepsilon^{i-1} u\, k^3\, (-\partial f_o/\partial\varepsilon)d\varepsilon}{1 + u^2B^2} \tag{3.36}$$

$$G_j = \frac{1}{3\pi^2 e^2} \int_0^\infty \frac{\varepsilon^{j-1} u^2 k^3\, (-\partial f_o/\partial\varepsilon)d\varepsilon}{1 + u^2B^2} \tag{3.37}$$

The forms of (3.36) and (3.37) suggest the definition of a new type of transport integral

$$L[g] = \int_0^\infty (-\partial f_0/\partial \varepsilon)\, g\,(\varepsilon, u, B) k^3\, d\varepsilon \qquad (3.38)$$

The transport integrals K_i and G_j can then be reexpressed in terms of L - integrals. Returning to the phenomenological eqs. (3.10) and applying eq. (3.38), we are also able to express the transport coefficients in terms of L-integrals. We will only show some results for two interesting cases, viz. in the limit of vanishing magnetic field and in the limit of strong magnetic field. The electron density can be specified as

$$n = \frac{1}{\pi^2} \int_0^\infty k^2 f_0 \, dk = \frac{1}{3\pi^2} L[1] \qquad (3.39)$$

and the electrical conductivity as

$$\sigma(0) = n\, e\, \mu = \frac{e}{3\,\pi^2}\, L[u] \qquad (3.40)$$

These two equations are suitable to demonstrate the difference between the conductivity mobility μ used by Harman and the mobility u : we find

$$\mu = L[u] / L[1]$$

So we may say that μ is the mobility u averaged over all occupied states.

The Seebeck and transverse Nernst coefficients in the limit of vanishing magnetic fields are given by

$$\alpha^i(0) = -\frac{k_o}{e} \left\{ \frac{L[xu]}{L[u]} - \eta \right\} \qquad (3.41)$$

$$N^i(0) = \frac{k_o}{eB^2} \left\{ \frac{L[x/u]\, L[1] - L[x]\, L[1/u]}{L^2[1]} \right\} \qquad (3.42)$$

In the limiting case of strong magnetic fields we obtain for the Seebeck coefficient

$$\alpha^{i}(\infty) = - \frac{k_o}{e} \{\frac{L[x]}{L[1]} - \eta\} \tag{3.43}$$

For extreme degeneracy ($\eta >> 1$) the Bethe-Sommerfeld representation of $L[g]$ can be applied

$$L[g] = (g\, k^3)_{\varepsilon=\varepsilon_F} + \frac{\pi^2}{6} (k_o T)^2 \left(\frac{\partial^2 (gk^3)}{\partial \varepsilon^2}\right)_{\varepsilon=\varepsilon_F} + \ldots\ldots\ldots \tag{3.44}$$

Taking into account (3.19) and (3.5) the quantity $u = \frac{e\tau}{m^*}$ becomes

$$u = u_o k^{2r-3} \left(\frac{d\varepsilon}{dk}\right)^2 \tag{3.45}$$

where u_o is a constant analogous to τ_o in eq. (3.19). Substituting the expression (3.45) in the equations (3.41) to (3.43), the following results are obtained for the coefficients $\alpha^{i}(\infty)$, $N^{i}(0)$ and $\alpha^{i}(0)$ in the case of strong degeneracy

$$\alpha^{i}(\infty) = - \frac{k_o}{e} \frac{\pi^{2/3}}{h^2} (k_o T) \frac{m^*}{(3n)^{2/3}} \tag{3.46}$$

$$N^{i}(0) = - \frac{1}{3} u_{\varepsilon_F} \left|\alpha^{i}(\infty)\right| \{2r - 6\gamma - 1\} \tag{3.47}$$

$$\alpha^{i}(0) = \frac{1}{3} \alpha^{i}(\infty) \{2r - 6\gamma + 2\} \tag{3.48}$$

The term $\gamma = \left(\frac{n}{m^*} \frac{dm^*}{dn}\right)_{\varepsilon=\varepsilon_F}$ gives the degree of non-parabolicity of the conduction band ; for a parabolic band $\gamma = 0$.

Since in strongly degenerate semiconductors only electrons in the vicinity of the Fermi level take part in the transport mechanism, the unaveraged mobility at the Fermi level u_{ε_F} can be replaced by the conductivity mobility μ . The last three formulae clearly show the influence of the scattering mechanism and the band structure on α^i and N^i, and also that $\alpha^i(\infty)$ is independent of the scattering mechanism. Eq. (3.46) affords a very convenient method of determining m^*. If measurements of $\alpha^i(\infty)$ are carried out on samples with different electron concentrations, the function $m^*(n)$ can be experimentally determined. After the determination of $m^*(n)$ the Seebeck and transverse Nernst coefficients can be used to obtain values for the scattering parameter r.

We now have to discuss the way in which $\alpha^i(\infty)$ can be determined experimentally, since mostly it is impossible to create such high magnetic field strengths that the Seebeck coefficient saturates completely. It has been shown[47] that $\Delta\alpha^i(B)$ can be presented as follows

$$\Delta\alpha^i(B) = \alpha^i(B) - \alpha^i(0) = \frac{k_o}{e} (k_o T) \frac{\pi^2}{3} \left(\frac{1}{u} \frac{du}{d\varepsilon} \frac{(uB)^2}{1+u^2B^2} \right)_{\varepsilon=\varepsilon_F}$$

Rewriting this as

$$\Delta\alpha^i(B) = \Delta\alpha^i(\infty) \frac{\mu^2 B^2}{1+\mu^2 B^2} \tag{3.49}$$

this extrapolation formula can be used to determine $\Delta\alpha^i(\infty)$ by plotting $B^2/\Delta\alpha^i(B)$ vs B . To verify this extrapolation method we calculated the dependence of $\mu^2B^2/\Delta\alpha^i$ on μ^2B^2 for typical values of r, P and Eg, on the basis of Harman's theory. The results are presented in Fig.4-16 of chapter 4 together with the experimental results. Another way of determining $\Delta\alpha^i(\infty)$ for strongly degenerate material, although less accurate, is given by the relation

$$\left|\Delta\alpha^i(\infty)\right| = \frac{N^i(0)}{\mu} \tag{3.50}$$

which equation can be easily verified with the aid of eqs. (3.46), (3.47) and (3.48). Hence, $\Delta\alpha^i(\infty)$ can in principle be obtained even when the available magnetic fields are only small.

The same kind of extrapolation formula seems to be valid for the thermal conductivity in a magnetic field

$$\Delta\kappa^{i}(B) = \Delta\kappa^{i}(\infty)\,\frac{\mu^2B^2}{1+\mu^2B^2} \tag{3.51}$$

Assuming that the lattice component of the total thermal conductivity is unaffected by the magnetic field, the relation between $\Delta\kappa^{i}(B)$ and B can be used to obtain $\Delta\kappa^{i}(\infty)$, which magnitude is equal to the electronic thermal conductivity $\kappa_E(0)$. This method of separating the electronic component from the lattice component of κ is particularly useful to determine the Lorenz number L. The magnitude of the experimentally determined Lorenz number compared with the theoretically expected value may give important information about the degree of inelasticity of the scattering mechanism (see section 3.4.).

As can be seen from eqs. (3.49) and (3.51) the intercepts of the straight lines $B^2/\Delta\alpha$ vs. B (and $B^2/\Delta k$ vs. B^2) yield values for the mobility μ. Two other ways of finding the mobility are given by the magnetic field dependences of the Righi-Leduc and transverse Nernst coefficients[48]. For the Righi-Leduc coefficients the following relation can be proved

$$-\frac{1}{S} = \frac{1 + \kappa_L/\kappa_E(0)}{\mu} + \frac{\kappa_L}{\kappa_E(0)}\,\mu B^2 \tag{3.52}$$

so that using the intercept and the slope of a straight line, values for μ and $\kappa_L/\kappa_E(0)$ can be found. The transverse Nernst coefficient gives once more a method of obtaining μ and $\Delta\alpha^{i}(\infty)$, by using the relationship

$$\frac{1}{N^{i}(B)} = \frac{1}{\left|\Delta\alpha^{i}(\infty)\right|}\left(\frac{1}{\mu} + \mu B^2\right) \tag{3.53}$$

3.4. Influence of inelastic scattering

The theory of transport phenomena based on the Boltzmann transport equation is only applicable if the scattering of the charge carriers is elastic, i.e. that one may apply the relaxation time approximation.

Korenblit and Sherstobitov[48] pointed out that if the scattering of electrons is partly inelastic due to interaction with longitudinal optical phonons, the transport effects can be calculated by assuming two complex relaxation times. In the case that $T \gtrsim \Theta_L/2$ (Θ_L is the Debije temperature for the longitudinal optical vibrations) the influence of the inelasticity on the transport coefficients in degenerate n-type semiconductors can be described by introducing the collision inelasticity coefficient s. The quantity s can also be expressed in terms of two mobilities [48,50] by

$$1 - s = \frac{\mu_T}{\mu_H} \tag{3.54}$$

where μ_H is the Hall mobility and μ_T the thermal mobility that is applicable when the material is subjected to a temperature gradient. In general, μ_T is smaller than μ_H if the scattering is inelastic, and the ratio μ_T/μ_H should be equal to L/L_o where L is the actual Lorenz number for the given degeneracy and scattering mechanism. Taking into account the inelastic scattering, eqs. (3.49) to (3.53) are changed in such a way that μ has to be replaced by μ_T. The formula (3.46) for the saturation value of the Seebeck coefficient remains unaltered, whereas (3.47) and (3.48) become

$$N^i(0) = -\frac{1}{3}\mu_T \left|\alpha^i(\infty)\right| \{ \frac{\mu_T}{\mu_H} (2r-6\gamma) - 1 \} \tag{3.55}$$

$$\alpha^i(0) = \frac{1}{3}\alpha^i(\infty) \{ \frac{\mu_T}{\mu_H} (2r-6\gamma) + 2 \} \tag{3.56}$$

Summarising we can say that, if the inelastic scattering is caused by collisions with optical phonons ($T \gtrsim \Theta_L/2$), the methods of determining the band structure described in section 3.3 remain applicable, provided we take into account two different mobilities.

CHAPTER 4

EXPERIMENTAL RESULTS AND DISCUSSION

In this chapter the main experimental results of the measurements on a number of cadmium arsenide samples with electron concentrations from about 0.7 to 13 × 10^{24} m^{-3} are presented and discussed. In the first section measurements of the temperature dependences of the resistivity, the Hall effect and the Seebeck effect of two characteristic samples are given. The sections which follow discuss in detail the measurements of the thermomagnetic effects : longitudinal and transverse Nernst effects, Righi-Leduc effect and Maggi-Righi-Leduc effect. These experimental results will be analysed by means of the theories reviewed in chapter 3. Finally, the thermal mobilities are compared with the Hall mobility of each sample, in order to get information on the inelastic contribution to the electron scattering mechanism.

4.1. Resistivity, Hall effect and Seebeck effect

In Figs. 4-1, 4-2 and 4-3 are shown the temperature dependences of the resistivity, the Hall coefficient and the Seebeck coefficient of two undoped samples of cadmium arsenide. The electron densities of the two samples are about 2 × 10^{24} m^{-3}, a typical value for undoped material. The results, i.e. a Hall coefficient which is virtually independent of temperature, and a resistivity and a Seebeck coefficient which increase linearly with the absolute temperature, indicate that there is only one type of strongly degenerate electrons. Formula (3.48) combined with (3.46) shows that, when the electron concentration (n), the electron scattering mechanism (r), and the form of the conduction band (γ) do not change with temperature, the linear dependence of $\alpha(0)$ on T is a good experimental test for strong degeneracy.

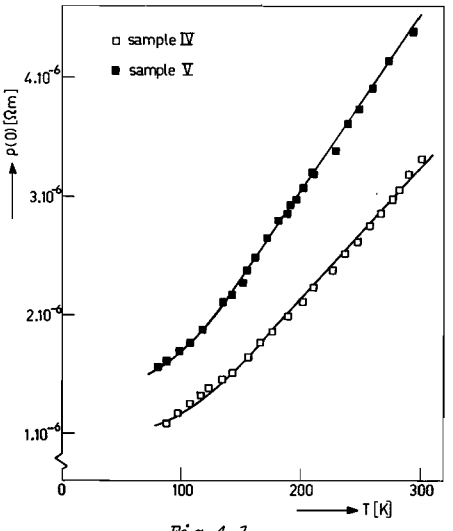

Fig. 4-1

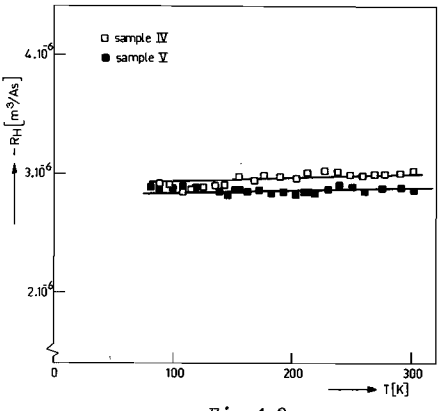

Fig. 4-2

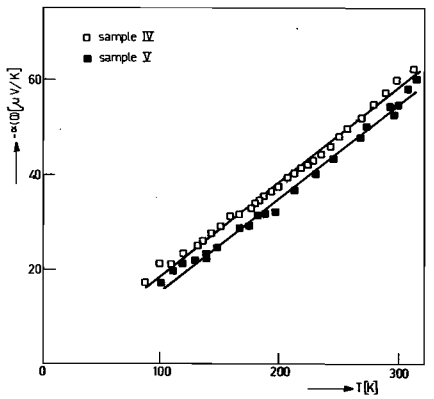

Fig. 4-3

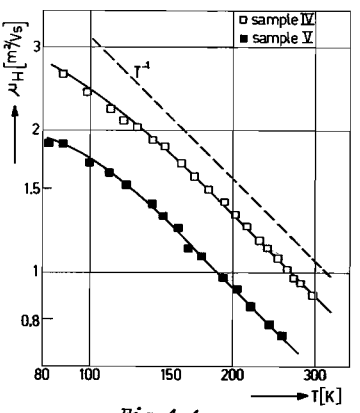

Fig. 4-4

Fig. 4-1 *Resistivities as functions of temperature for two undoped samples of Cd_3As_2 with electron concentrations of about 2×10^{24} m^{-3}.*

Fig. 4-2 *Hall coefficients as functions of temperature.*

Fig. 4-3 *Zero-field Seebeck coefficients as functions of temperature.*

Fig. 4-4 *Hall mobilities as functions of temperature.*

The variation of the experimental Hall mobility with temperature is shown in Fig.4-4. As can be seen from this figure, the temperature dependence of the mobility is approximately T^{-1} over most of the temperature range, which may be due to scattering by acoustical phonons[51] as well as by optical phonons[52]. At low temperatures the curves μ_H vs. T diverge from the line T^{-1}, indicating the presence of an additional scattering mechanism, probably due to impurities.

The measurements of the Hall coefficient and the resistivity are used to determine values of the Hall mobility and the electron concentration according to the relations

$$\mu_H = \frac{-R_H}{\rho(0)} \tag{4.1}$$

and

$$n = \frac{-1}{eR_H} \tag{4.2}$$

However, at this point we have to discuss first the validity of this procedure of determining n,since, if relation (4.2) is used, it is assumed that the Hall mobility μ_H is equal to the conductivity mobility μ. The correct expression for the electron concentration reads

$$n = -\frac{\mu_H/\mu}{eR_H} \tag{4.3}$$

in which the ratio μ_H/μ is greater than 1. The value of μ_H/μ depends on the degree of degeneracy of the electron gas, the scattering mechanism and the conduction band structure. Only for extreme degeneracy ($\eta\to\infty$) does the numerator of (4.3) exactly equal 1, independent of the scattering mechanism and band structure. In case a parabolic band applies, in first approximation the ratio μ_H/μ is given by

$$\frac{\mu_H}{\mu} = 1 + \frac{\pi^2}{3\eta^2}(r-\tfrac{1}{2})^2 \tag{4.4}$$

from which it can be seen that for strongly degenerate material ($\eta \gtrsim 5$) the expression is nearly equal to 1. If a non-parabolic conduction band applies,

no such simple expression is available, since in this case μ_H/μ is also dependent on the band gap E_g. Calculations by Harman[53] show that, if the electrons in a Kane band are scattered by optical phonons and if $\eta \gtrsim 4$, the Hall mobility is equal to the conductivity mobility within a few per cent.

Summarising, we may conclude that the electron density can be obtained accurately enough from the value of R_H and that the Hall mobility μ_H is equal to the conductivity mobility μ. The latter fact makes it possible to compare the experimentally observed magnetic field dependences of the thermomagnetic transport coefficients on $\mu_H B$ with the theoretical predictions of the dependences on μB. Note that in the theory of Korenblit and Sherstobitov (section 3.4) it has been assumed tacitly that the conductivity mobility may be replaced by the Hall mobility (or by the thermal mobility in case of partially inelastic scattering).

Table 4-1 gives the values of the electron concentrations and Hall mobilities of a number of samples used in our experiments. The doping elements in the different samples are also included in the table.

Table 4-1

sample	I	II	III	IV	V	VI	VII	VIII†
doping element	Au	Au	Au	-	-	-	Ga	S
n (10^{24} m^{-3})	0.75	0.85	0.73	2.05	2.20	2.41	6.45	13
μ_H (m^2/Vs) $T \approx 300$ K	1.60	1.44	1.49	0.90	0.78	1.02	0.60	0.3
μ_H (m^2/Vs) $T \approx 80$ K	4.32	3.51	4.18	2.25	1.80	-	1.42	-

† *A remark should be made concerning sample VIII. The S-doped material is in general so brittle that it is hardly possible to obtain a sample with dimensions suitable for carrying out thermomagnetic measurements with reasonable accuracy. The dimensions of sample VIII are only 8 × 2 × 2 mm, whereas the others have dimensions of about 25 × 5 × 5 mm. Such small dimensions render the results inaccurate.*

Remarks on R_H and $\rho(0)$

The Hall coefficient and the resistivity can also be defined in two ways: under isothermal and under adiabatic conditions.
The symbols R_H and $\rho(0)$ used in this thesis always refer to the isothermal coefficients. If R_H and $\rho(0)$ are measured by means of a direct current through the sample, in principle corrections should be made for the Ettingshausen effect (on R_H) and the Peltier effect (on $\rho(0)$). Although the Ettingshausen and the Peltier effects have not been measured in our samples, the magnitudes of these effects can be derived from the Bridgman and Kelvin relations, respectively

$Q\kappa = N\,T$

$\pi = \alpha T$

where Q is the Ettingshausen coefficient and π the Peltier coefficient.
If necessary, R_H and $\rho(0)$ are corrected for these effects; moreover in some cases measurements have been carried out with alternating current, in which case the thermal effects are eliminated.

4.2. *Seebeck effect in a magnetic field (longitudinal Nernst effect)*

4.2.1. Measurements of $\Delta\alpha^{i}(B)$.

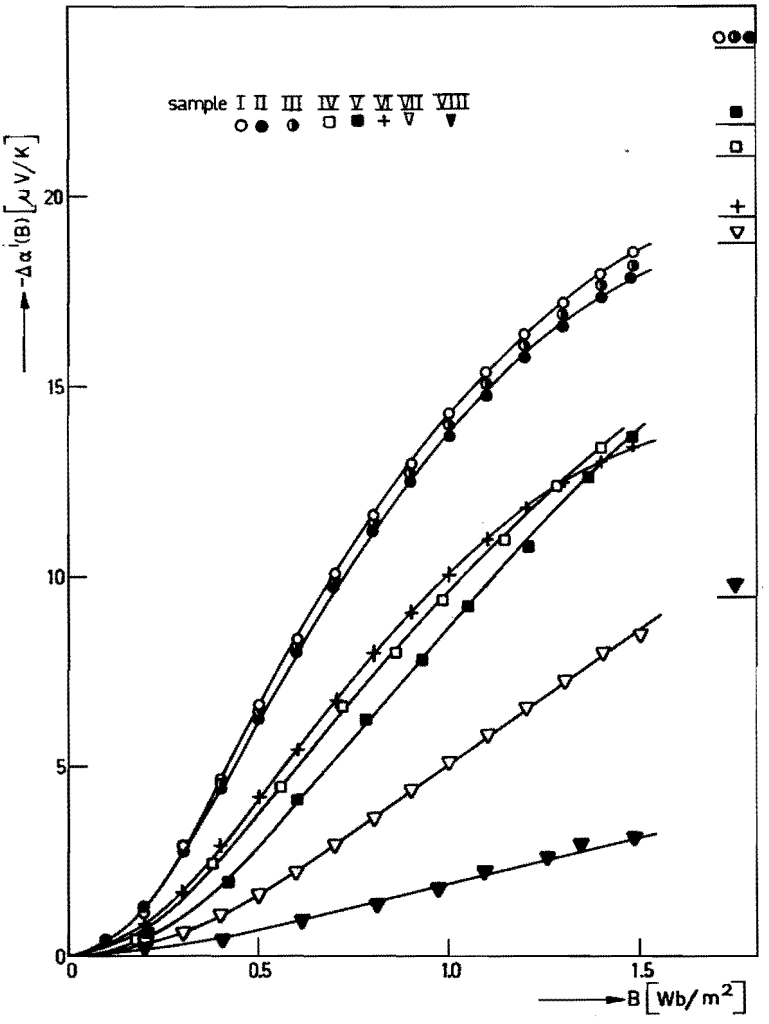

Fig. 4-5 Variations of the isothermal Seebeck coefficients with magnetic induction at room temperature for a number of samples.

Fig.4-5 gives the variations of the isothermal Seebeck coefficients with magnetic induction for a number of samples at room temperature. Starting with parabolic shapes, the curves pass gradually into linear parts and at the highest magnetic fields show a weak tendency to become horizontal. This deviation from the straight line is the more pronounced as the mobility of the sample is higher. However, the applied magnetic field strengths are far too low to determine the saturation values of the Seebeck coefficients directly from these curves. At low temperatures (see Fig. 4-6) the experimental values of $\Delta\alpha^i(B)$ at the highest values of B are much closer to their saturation values, because of the much higher mobilities of the samples at these temperatures. Even in the latter case, determining $\Delta\alpha^i(\infty)$ from the curves would still be very inaccurate for the samples with lowest μ . In order to show the importance of this remark, the saturation values $\Delta\alpha^i(\infty)$ as found in the more accurate way, have been marked on the right hand sides of both Figs. 4-5 and 4-6.

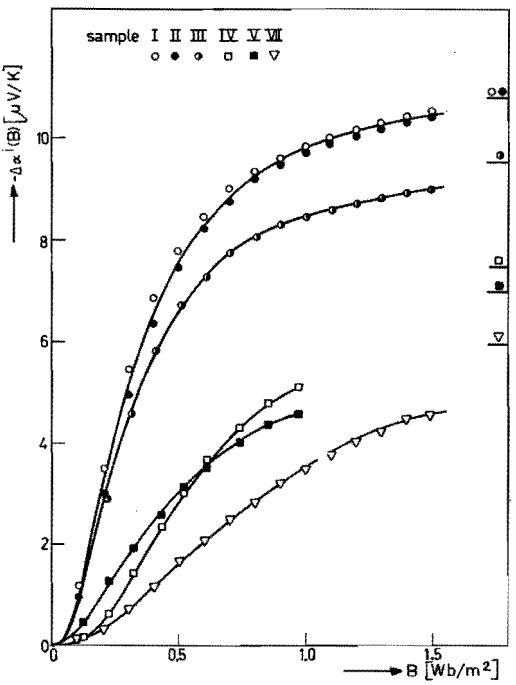

Fig. 4-6 As Fig. 4-5, at liquid nitrogen temperature.

In Figs. 4-7 and 4-8 the quantities $B^2/\Delta\alpha^i(B)$ have been plotted as functions of B^2 for the measurements at room temperature and at liquid nitrogen temperature, respectively. The points for each sample lie rather well on a straight line, so the use of the extrapolation method based on eq. (3.49) seems justifiable.

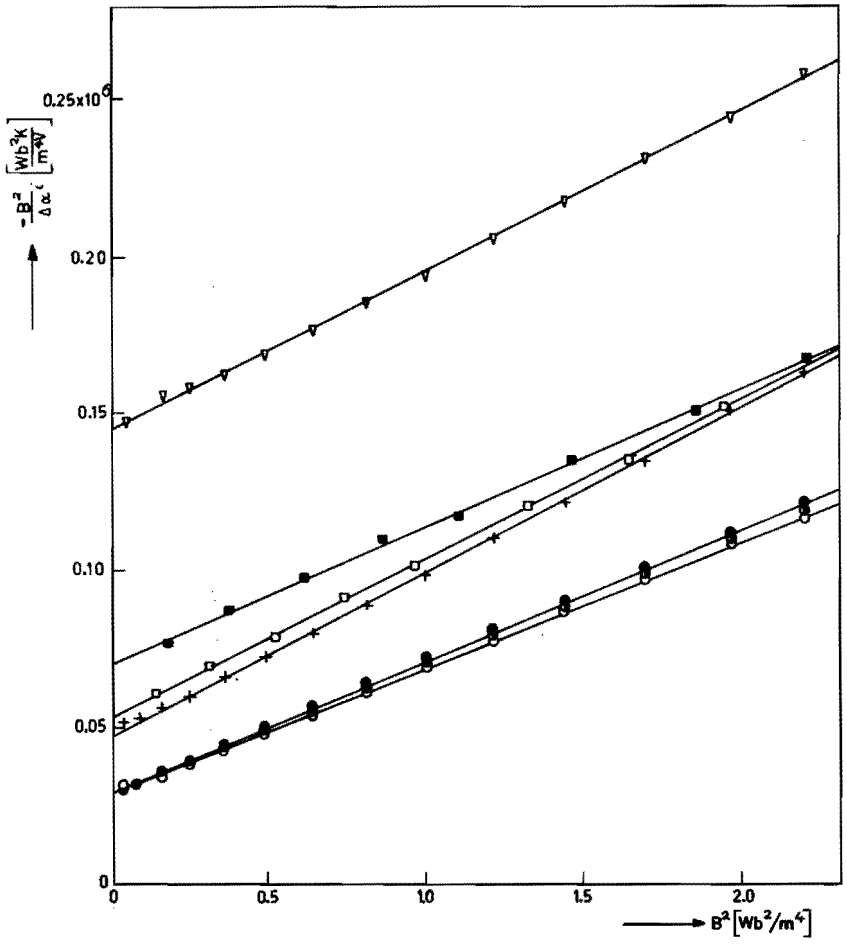

Fig. 4-7 Extrapolation graphs for the determination of the saturation values of the isothermal Seebeck coefficients $\alpha^i(\infty)$ and the thermal mobilities μ_T, at room temperature.

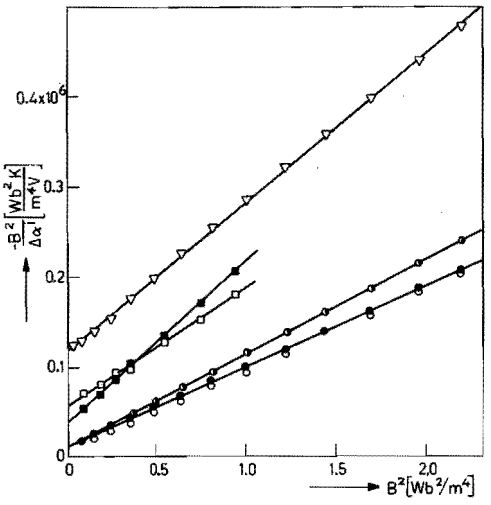

Fig. 4-8 Extrapolation graphs at liquid nitrogen temperature.

4.2.2. Concentration dependence of the effective mass; Kane band model.

Having determined the values of $\Delta\alpha^i(\infty)$ by the extrapolation method, we are now able to calculate the corresponding values of the electron effective masses by substituting n (obtained from the Hall effect), $\alpha^i(\infty)=\alpha^i(0)+\Delta\alpha^i(\infty)$ and T (the average temperature) in eq. (3.46). Carrying out these calculations we find an electron effective mass which increases from 0.033 m_o to 0.076 m_o with electron concentration increasing from 0.75 to 13 $\times 10^{24} m^{-3}$, a result which cannot be explained by the assumption of a single parabolic conduction band. If we plot the room temperature values of $\left(\frac{m^*/m_o}{1-m^*/m_o}\right)^2$ vs. $n^{2/3}$, we obtain a number of points which fit a straight line (Fig. 4-9). As has been shown by eq. (3.35), such dependence of the electron effective mass on concentration implies the applicability of Kane's non-parabolic conduction band model.

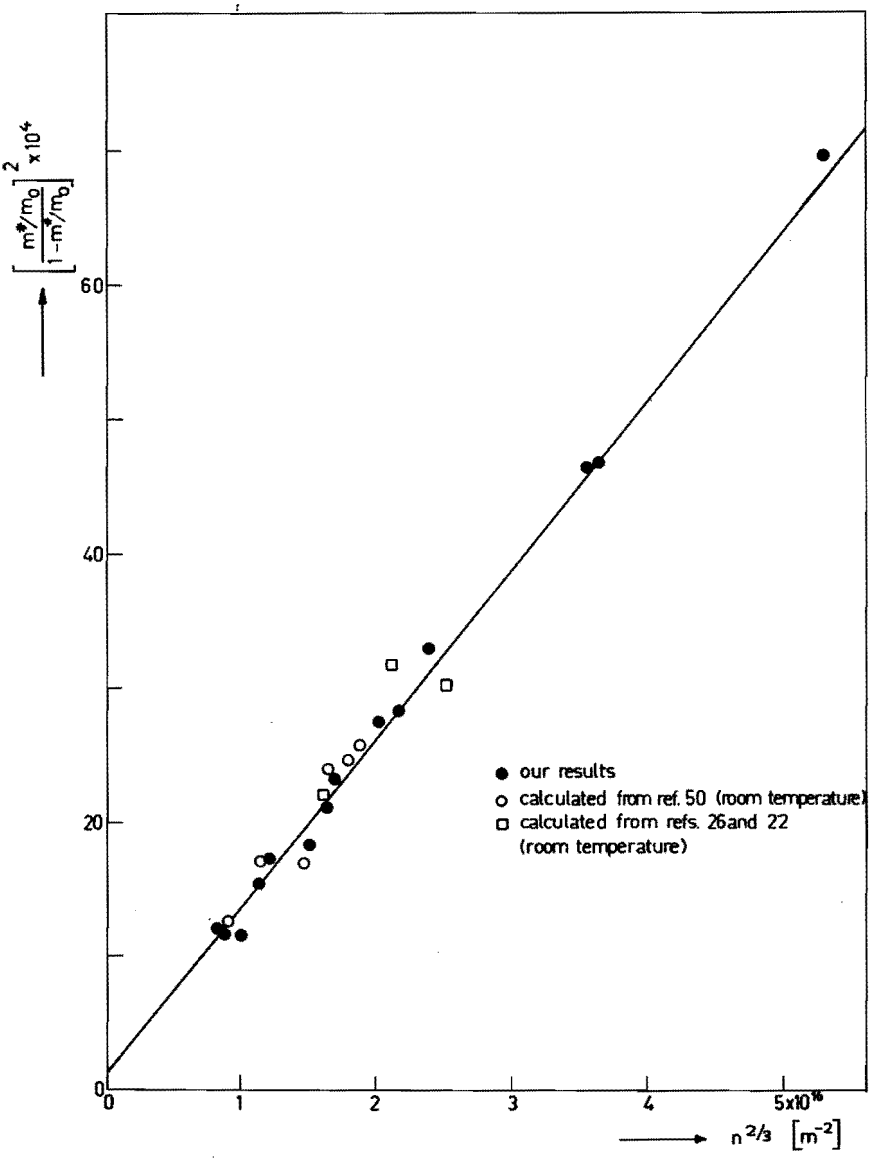

Fig. 4-9 *The dependence of the electron effective mass in cadmium arsenide on concentration, at room temperature.*

From the slope of the line we calculated P to be equal to 13×10^{-29} Jm, or, expressed in units frequently found in the literature, $P = 8.1 \times 10^{-8}$ eVcm. Using this value in the first term of the right-hand side of (3.35), we obtain from the intercept of the line a value of $E_g = 0.15$ eV for the band gap of $Cd_3 As_2$.

Before discussing these results we will first pay attention to the low temperature measurements. Unfortunately, the number of samples investigated at low temperatures is too small for a graph similar to the one in Fig.4-9 to be constructed. Therefore we would prefer to confine ourselves to comparing our results with those reported in the literature. Thus, in Fig.4-10 our results and those of Rosenman[29] have been compared with the dependence of m^*/m_o on $n^{1/3}$ at 80 K found by Armitage and Goldsmid[28,50] (line through dotted points). The equation of the line m^*/m_o vs. $n^{1/3}$

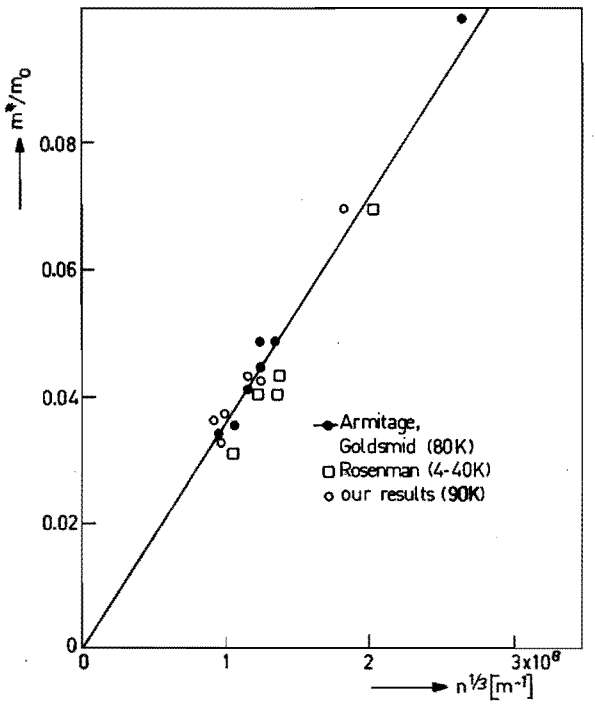

Fig. 4-10 The dependence of $\frac{m^*}{m_o}$ *on* $n^{1/3}$ *at liquid nitrogen temperature, reported by Armitage and Goldsmid*[28,50].

through the origin is a simplified form of eq. (3.35), if it is assumed that E_g is very small, and if m^*/m_o is neglected with respect to 1. Although our points do not fit completely the straight line, yet they may be considered as a confirmation of the results of Armitage and Goldsmid. Concerning the points of Rosenman, which lie somewhat below the line, it should be mentioned that these measurements were carried out on single crystals at liquid helium and liquid hydrogen temperatures, with the magnetic induction parallel to the c-axis of the crystals. As we noticed in Chapter 1, the effective mass $m^*_{||}$ is smaller than $m^*_{\perp}$, so it becomes evident that the values of m^* measured on polycrystalline samples (Armitage and Goldsmid as well as we used polycrystalline samples) must be greater than $m^*_{||}$.

Let us now compare our values of P with those reported by other authors, who also assumed that the conduction band of Cd_3As_2 can be described by the Kane band model. The investigations by Armitage and Goldsmid mentioned above, yielded a value of P equal to 8.3×10^{-8} eVcm. Taking into account the experimental inaccuracy and the fact that P might be slightly dependent on the temperature, we may say that the agreement between this value and ours (8.1×10^{-8} eVcm) is almost perfect. Armitage and Goldsmid were not able to determine a value of E_g directly from their measurements of m^* vs. n, since they assumed that the first term in the right-hand side of eq. (3.35) could be neglected. Using the values of the Fermi level and the saturation value of the Seebeck coefficient for the sample with lowest electron concentration, they estimated that E_g and $m^*(0)$ (this quantity will be introduced below) should be less than 0.1 eV and 0.01 m_o, respectively.

Two other quantities which are often used in the literature[54] as characterising parameters of a Kane type conduction band, are the effective mass at the bottom of the band $m^*(k=0)$, or shortly $m^*(0)$, and the parameter Q. Using $m^*(0)$ and Q instead of E_g and P leads to the following alternative form of eq. (3.35)

$$\left[\frac{m^*/m_o}{1-m^*/m_o}\right]^2 = \left[\frac{m^*(0)}{m_o}\right]^2 + \frac{2\hbar^2}{m_o Q}(3\pi^2 n)^{2/3} \qquad (4.5)$$

in which Q is equal to $\dfrac{E_g}{m^*(0)/m_o}$ or expressed in P, $Q = \dfrac{4m_o P^2}{3\hbar^2}$.

Analysing Fig.4-9 in terms of this equation, we obtain the results : $m^*(0) = 0.012\ m_o$ and Q = 12.5 eV at room temperature. The measurements of Rosenman at liquid helium temperatures referred to above, yielded a value of Q = (15 ± 2) eV. These studies were not accurate enough to determine the value of $m^*(0)$, so that in order to compare our value of $m^*(0)$ with others we only have the disposal of the maximum value $m^*(0) = 0.01\ m_o$ estimated by Armitage and Goldsmid.

An important point which has not yet been discussed is the fact that the magnitude of P, found from the concentration dependence of the effective mass, depends on the spin-orbit splitting energy of the valence band Δ_{so}, which is unknown for Cd_3As_2. Our analysis, as those of the authors cited, are based on a Kane band given by eq. (3.29). However, this equation is only valid if the spin-orbit splitting is much larger than the band gap. For an arbitrary spin-orbit splitting, eq. (3.29) changes into[55]

$$\varepsilon = \frac{\hbar^2 k^2}{2m_o} - \frac{|E_g|}{2} + \frac{1}{2}\left(E_g^2 + a\,P^2k^2\right)^{1/2} \qquad (4.6)$$

where a denotes the influence of the spin-orbit splitting. For infinite spin-orbit splitting $a = \frac{8}{3}$ and the equation becomes identical with (3.29); if Δ_{so} is small compared with E_g, a equals 4.

Wagner et al.[33a] analysed their measurements of the magneto-absorption in $Cd_xZn_{3-x}As_2$ by assuming a Kane band model with a = 4, and found that $P = 8.1 \times 10^{-8}$ eVcm for all samples with $2.6 < x < 1.3$, whereas E_g varied from 0.02 eV for x = 2.6 to 0.42 eV for x = 1.3. If E_g continues to decrease with increasing x, as is the case in the $Cd_xHg_{1-x}Te$ system, the direct band gap of Cd_3As_2 would be "negative", implying the applicability of the α-Sn or HgTe band structure for cadmium arsenide. Using this model, the magneto-optical data of Haidemenakis et al.[26] have been analysed by Wagner et al., which resulted in $P = 9.1 \times 10^{-8}$ eVcm, $E_g = 0.38$ eV for cadmium arsenide.

The assumption that the spin-orbit splitting of Cd_3As_2 is small compared with the band gap, however, seems disputable. The magnitude of this quantity is still unknown, but if we make a rough estimate from the spin-orbit splittings of the isolated Cd and As atoms, a value of about 0.4 eV results, which is not small compared with E_g, even not if the value of $E_g = 0.38$ eV were correct. If we assume that $a = \frac{8}{3}$ instead of 4, the value of P reported by Wagner et al. becomes 11×10^{-8} eVcm, which deviates

considerably from the values discussed earlier in this section.

Up to now we have only discussed the agreement between the values of P for cadmium arsenide. However, it is also interesting to compare P for Cd_3As_2 with the values of P reported for other semiconducting compounds obeying a Kane band model. The value of P was found to be nearly the same for all investigated III-V-compounds, viz. 8.5×10^{-8} eVcm, a result from which Ehrenreich[56] suggested that P might be regarded as a constant for these compounds. Recent investigations on the II-VI-compounds HgTe and HgSe proved that these materials possess a Kane conduction band with $P = 8.3 \times 10^{-8}$ eVcm for both compounds[57], thus also close to the average value for III-V-compounds. It appears that, apart from the result reported by Wagner et al., within experimental accuracy, the value of P for cadmium arsenide is also in good agreement with the value in question. This is the more interesting because the III-V-compounds as well as the compounds HgTe and HgSe possess the zincblende structure, whereas Cd_3As_2 has a tetragonal unit cell. The salient feature arises here that the properties of a material with a tetragonal crystal structure have been interpreted in terms of a band model which was originally developed for a cubic crystal lattice (InSb), a contradiction to which no attention has been paid in the literature. We believe that an answer to the question why the conduction band structure (and the semiconducting properties in general) of Cd_3As_2 resemble so much those of the zincblende structures, would be found by carefully studying the basic physico-chemical properties which make a material a semiconductor. A point of contact to this idea we find in the work of Goryunova[58]. This author studied the chemistry and the formation of semiconducting compounds in order to explain existing classes and to predict new classes of semiconducting compounds. For this purpose she distinguished between different crystallo-chemical groups : normal tetrahedral phases with an average of four valence electrons per atom, defect and excess tetrahedral phases with an average of more or less than four electrons per atom, respectively. From Goryunova's point of view Cd_3As_2 might be regarded as an excess tetrahedral phase (3.2 electrons per atom), in which three quarters of the tetrahedral vacancies formed by the cubic close-packed As-ions are occupied by Cd-ions. In the zincblende structure (normal tetrahedral phase) the metal ions occupy half of the tetrahedral vacancies formed by the cubic-close-packed non-metal sublattice.
The unit cell of Cd_3As_2 would then be tetragonal, only because of the

ordering of the vacant and occupied tetrahedral sites, so that the tetragonal crystal structure would become irrelevant. It is difficult to examine to what extent Goryunova's postulates are correct; in addition, the discovery of the high electron mobility and other InSb-like properties of $CdSnAs_2$ (chalcopyrite structure)[35] seems to support these ideas.

So far the discussion of the results obtained from Fig.4-9 has been mainly restricted to the parameter P. A discussion of the value of E_g reported by us, will be postponed until more experimental results have been given.

4.2.3. Scattering mechanism

From the relation between the zero-field and the saturated Seebeck coefficients (eq. (3.48)) the scattering mechanism can be obtained. For that purpose however, we should determine first the non-parabolicity parameter γ. The dependence of m^* on n is completely determined by the straight line in Fig.4-9, so the equation of this line can be used to calculate $\gamma = \frac{n}{m^*} \frac{dm^*}{dn}$.
Writing eq. (3.35) as

$$\left[\frac{m^*/m_o}{1-m^*/m_o} \right]^2 = A^2 + C\, n^{2/3} \qquad (4.7)$$

it can be proved that, by differentiating the left and right-hand sides with respect to n, γ becomes

$$\gamma = \frac{1}{3}\, C\, n^{2/3}\, \frac{(1-m^*/m_o)^3}{(m^*/m_o)^2} \qquad (4.8)$$

where $C = \frac{21.40 \times 10^{-76}}{p^2}$, and m^* is still dependent on n. The result of these calculations is plotted in Fig.4-11 as γ vs $n^{2/3}$. The inset of the figure shows a similar curve reported by Shalyt et al.[59] for HgSe.
Within the investigated range of electron concentrations γ is practically

independent of n and nearly equal to 0.3. The curve also shows that γ becomes zero for very low concentrations, since at the bottom of a Kane band the $\varepsilon(k)$ relation becomes parabolic. It can also be seen that γ is less than $\frac{1}{3}$, the maximum value predicted by theory.

With the value of γ from Fig.4-11 and the ratio between $\alpha^{i}(\infty)$ and $\alpha(0)$ for each sample, the value of the scattering parameter r can be obtained. The results are shown in Fig.4-12, from which it appears that over the whole investigated range of concentrations r equals 1. The fact that r equals 1, means that, if $T > \Theta_L$ (Θ_L is the Debije temperature for longitudinal optical phonons), polar scattering due to optical phonons is the dominant mechanism [43,52,60].

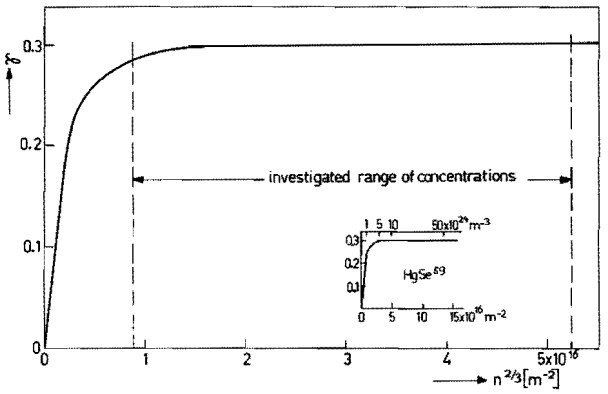

Fig. 4-11 The non-parabolicity parameter as function of electron concentration at room temperature.

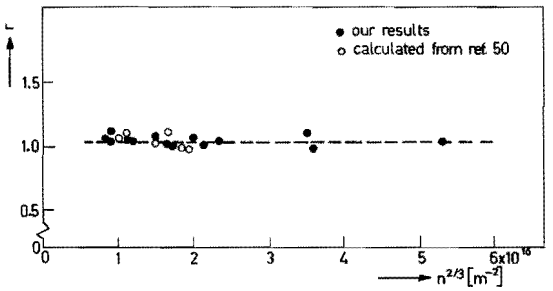

Fig. 4-12 The scattering parameter for different samples at room temperature.

The condition $T > \Theta_L$ is an essential one, since at lower temperatures this scattering mechanism is in general not elastic, so that the solution of the Boltzmann equation by means of a single relaxation time is no longer possible. In order to verify if this condition is fulfilled in cadmium arsenide, the Debije temperature has been determined from measurements of the specific heat in the temperature range of 2.5 to about 25 K[§] . These measurements yield a value of Θ_o = 164 K, where Θ_o is the extrapolated value of the Debije temperature at absolute zero. However, the expected low-temperature T^3-dependence of the specific heat occurs only at temperatures up to about 3 K. The Debije temperature Θ, calculated from the observed

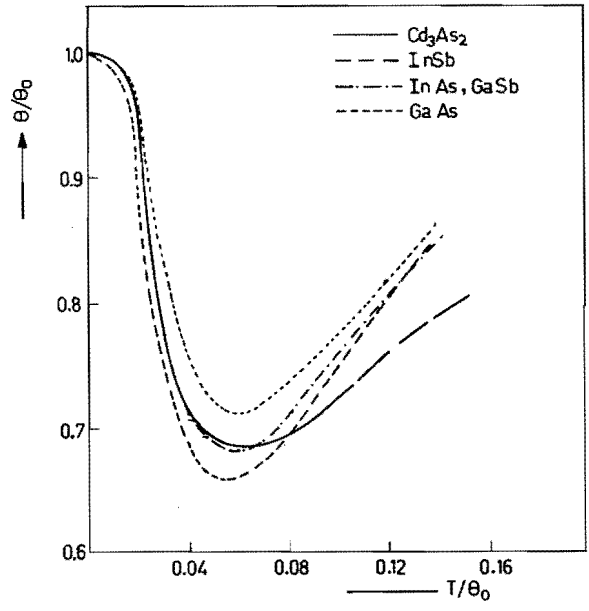

Fig. 4-13 A graph of the reduced Debije temperature of Cd_3As_2 as function of reduced temperature. The curves for the III-V-compounds are taken from refs. 61 and 62.

---

§ *Thanks are due to Mr. Ir. A.J. van der Steld and Mr. Ir. J. Th. Heessels for carrying out these measurements.*

specific heat, the actual experimental temperature and the Debije function, shows a rapid decrease with increasing temperature to a minimum of about 115 K at about 10 K. In Fig.4-13 a graph is given of the reduced Debije temperature as a function of the reduced temperature, which shows that both location and depth of the curve for Cd_3As_2 are in good agreement with those observed for a number of III-V-compounds. In the case of the III-V-compounds this dip is in agreement with the results from the lattice absorption bands in the infrared. We feel justified in assuming that the frequency distribution of the lattice vibrations in Cd_3As_2 is similar to those in the III-V-compounds, which means that the Debije temperature for the longitudinal optical phonons does not deviate much from the value of Θ_o. Assuming this magnitude of Θ_L, we expect that at room temperature ($T \simeq 2\Theta$)the scattering mechanism is almost completely elastic, whereas at liquid nitrogen temperature ($T \simeq \Theta/2$) the scattering mechanism contains an inelastic contribution, and the transport phenomena should be described by the two-relaxation time theory of Korenblit and Sherstobitov. For comparison, it should be noted that the Debije temperatures Θ_o of InSb, HgSe and HgTe (the materials whose transport properties resemble so much Cd_3As_2) are reported to be 206, 137 and 114 K, respectively [61,63].

Finally, we would make a further remark concerning the partially inelastic scattering of the electrons. The values of μ_T have been determined from the slopes and the intercepts of the straight lines in Fig.4-7. They will be presented in section 4.5, together with the values of μ_T/μ_H and L/L_o obtained from the magnetic field dependences of the thermal conductivities and Righi-Leduc coefficients. Anticipating the results presented later on, we would remark that at room temperature differences are observed between μ_T and μ_H, only for the samples with the lowest electron concentrations (I, II and III). Instead of using eq. (3.48), the equivalent eq. (3.56) has been used to determine the values of r for these samples.

4.2.4. Comparison with theoretical predictions

In order to compare the variations of the Seebeck coefficients with magnetic field with theoretical calculations based on Harman and Honig's theory (section 3.2), we would first determine the values of the reduced Fermi levels for the different samples. Taking the room temperature values

of $P = 13 \times 10^{-29}$ Jm and $E_g = 0.15$ eV (or a reduced energy gap $x_g = 6$) from Fig.4-9, the relation between the electron concentration n and the reduced Fermi level η can be calculated from eq. (3.31). As can be seen in Fig.4-14, an electron concentration increasing from about 0.75 to 13×10^{24} m^{-3} corresponds to a value of η increasing from about 4 to 16. The values of η for the Au doped samples (I, II, III), the undoped samples (IV, V, VI), the sample VII, and the sample VIII appear to be about 4, 8, 12 and 16, respectively.

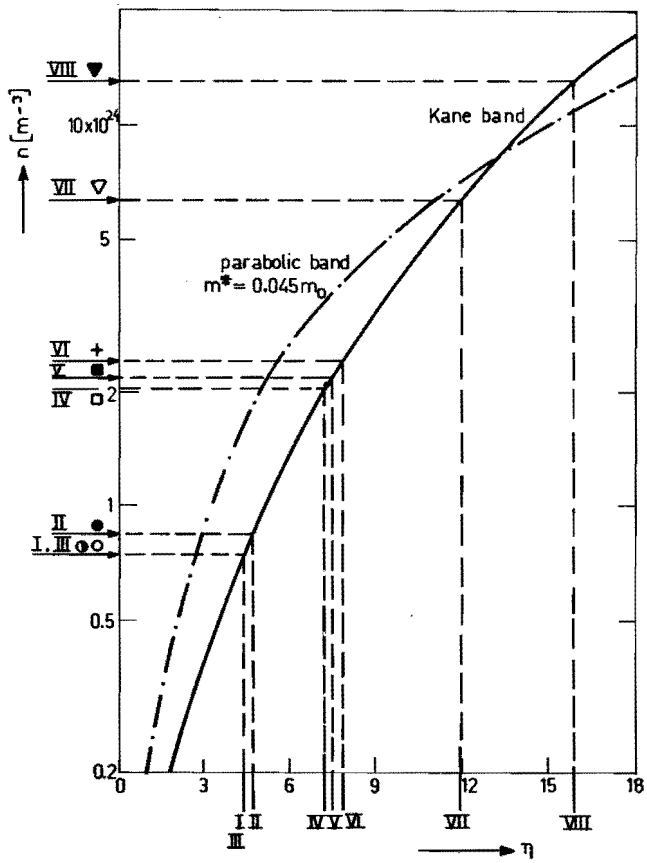

Fig.4-14 The relation between the electron concentration and the reduced Fermi level for a Kane-type conduction band ($P = 8.1 \times 10^{-8}$ eVcm; $x_g = 6$; $T = 300$ K).

At this point we would make some remarks concerning the values of the reduced Fermi levels of Cd_3As_2 samples at room temperature as reported by Ballentyne and Lovett[5,22] and Zdanowicz[15]. For samples with an electron concentration of about 2×10^{24} m^{-3} these authors reported a value of $\eta \simeq 4$, whereas we obtain a value of 7-8 for samples with corresponding concentrations. The reason for this discrepancy is to be found in the different ways of determining η. In refs. 15 and 22 the values of η were obtained from the zero-field Seebeck coefficients, with the assumptions of a single parabolic conduction band and scattering by acoustical phonons. Actually this procedure of determining η is in this case similar the determination of the dependence of n on η for a parabolic band with $m^* \simeq 0.045\ m_o$ (the value of m^* for samples with $n \simeq 2 \times 10^{24}$ m^{-3}). For the sake of illustration, this dependence has been plotted also in Fig.4-14, which shows clearly that for samples with $n \simeq 2 \times 10^{24}$ m^{-3} there is a considerable difference between the values of η determined from the two procedures.

Since a value of η can now assigned to each sample we are able to compare the experimental results with the numerical results calculated by means of the theory outlined in section 3.2. A graph of the relative variations of the isothermal Seebeck coefficients $\frac{\Delta\alpha\ (B)}{\alpha(0)}$ vs. μB at room temperature is given in Fig.4-15, together with the theoretical curves for a Kane band with $P = 8.1 \times 10^{-8}$ eVcm, $x_g = 6$ and four relevant values of η. For the same values of the parameters, the theoretical relations between $\frac{\mu^2 B^2}{\Delta\alpha/\alpha(0)}$ and μ^2B^2 are plotted in Fig.4-16. Both in Figs.4-15 and 4-16 the experimental points of the different samples fit very well the corresponding theoretical curves. Moreover, Fig.4-16 shows once more that the extrapolation method of determining $\Delta\alpha^i(\infty)$ is justifiable for a Kane band model with a single type of charge carriers. Because of the low mobility of sample VIII, the experimental points in Fig.4-15, and particularly in Fig.4-16, cover only narrow ranges of μB and μ^2B^2 values. Moreover, the agreement with the theoretical curves for $\eta = 16$ is not so good as for the other samples, which we will ascribe to the inaccuracies of the measurements of this sample mentioned earlier in section 4.1. Regarding the experimental values of μ it should be mentioned that for the samples I, II and III, we used the thermal mobility μ_T, whereas for the other samples it makes no difference which value is used, μ_T or μ_H.

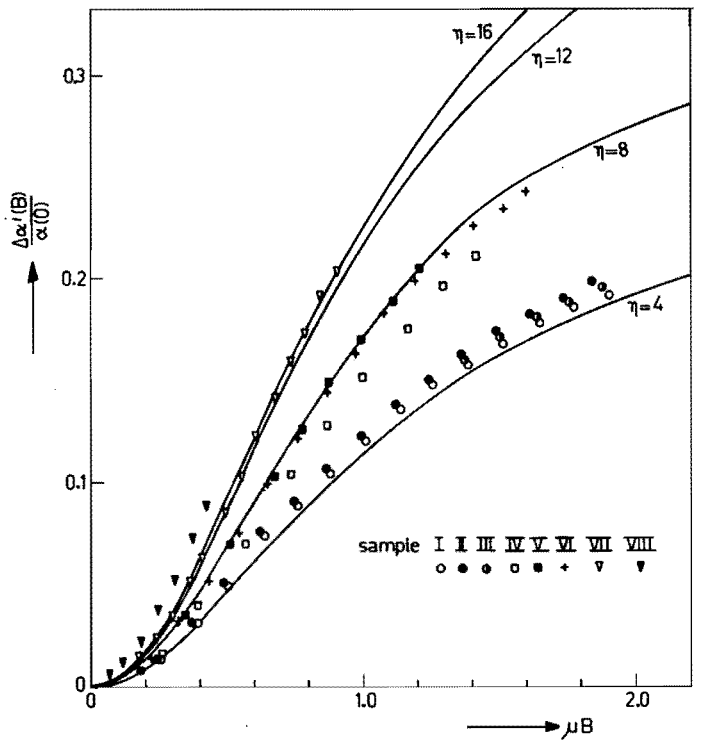

Fig. 4-15 Experimental and theoretical values of the relative variations of the Seebeck coefficients with μB at room temperature.

The theory of Harman and Honig offers the possibility of predicting not only the magnetic field dependence of α^i, but also the variation of the zero-field Seebeck coefficient $\alpha(0)$ with n. Since $\alpha(0)$ is insensitive to the value of x_g, the measurements of this coefficient as a function of n can also be used to determine the scattering mechanism. Using a simple measuring equipment[34], we determined $\alpha(0)$ for a large number of samples with highly different electron concentrations. The results are shown in Fig. 4-17 together with the theoretical curves for a Kane band ($P = 8.1 \times 10^{-8}$ eVcm, $x_g = 6$) and three different scattering mechanisms; the experimental points fit very well the curve for optical phonon scattering. The measurements and their theoretical explanation (a two-band model with

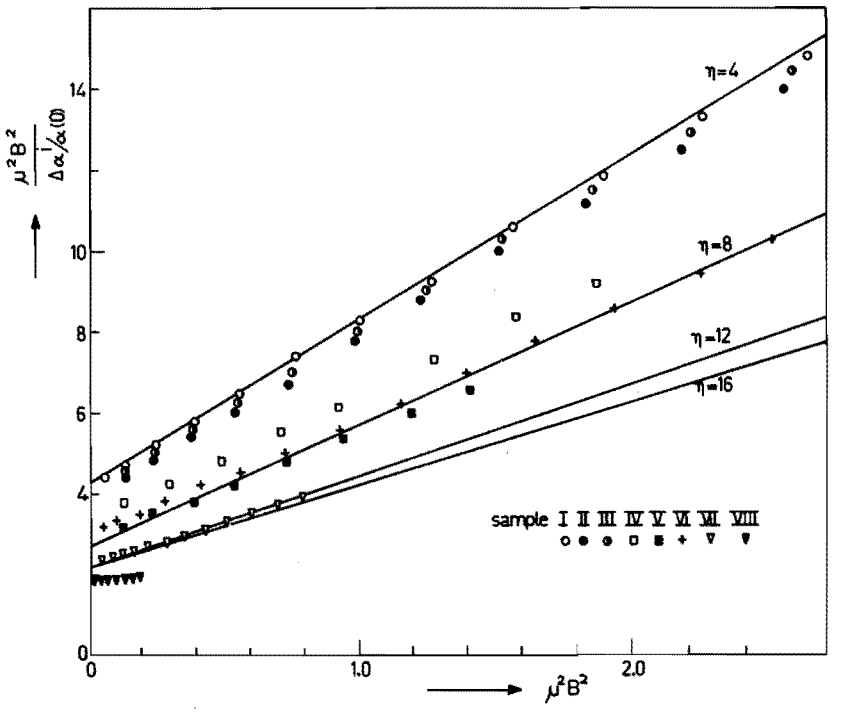

Fig. 4-16 Comparison of experimental and theoretical extrapolation graphs.

acoustical lattice scattering) reported by Shevchenko et al.[24], are also shown in the figure. Irrespective of the large spread we conclude that their experimental result roughly fit ours, and that neither shows the necessity of a two-band model.

Summarising the results discussed in this section we conclude that the room temperature Seebeck coefficient of Cd_3As_2 within and without a magnetic field can be well explained quantitatively by assuming a Kane band model and scattering by polar optical phonons. From theoretical curves (not shown in this thesis), calculated for values of x_g and r different from those used in Figs. 4-15 and 4-17, it appears that the curves $\frac{\Delta\alpha^1(B)}{\alpha(0)}$ vs. B and $\alpha(0)$ vs. n are highly sensitive to the magnitude of r, but rather

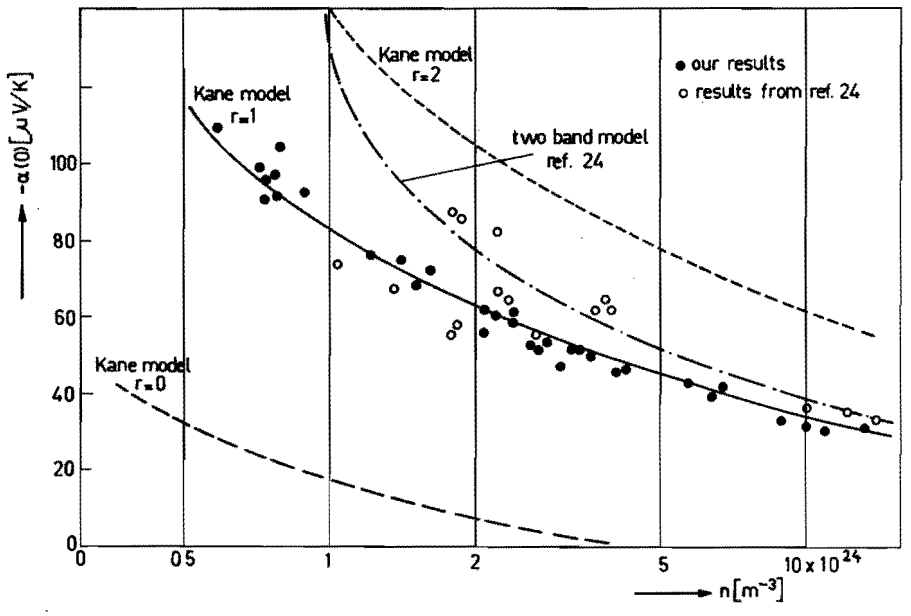

Fig. 4-17 The concentration dependence of the zero-field Seebeck coefficient.

insensitive to E_g. So, judging by the measurements of the Seebeck effect, there is no doubt about the nature of the scattering mechanism at room temperature. However, it is difficult to deduce an accurate value of E_g from these measurements (N.B. Values of E_g between 4 and 8 still give curves which are reasonably in agreement with the experimental points).

4.3. *Thermal conductivity in a magnetic field (Maggi-Righi-Leduc effect)*

4.3.1. Measurements of $\kappa(0)$

The results of the measurements of the total thermal conductivity $\kappa(0)$ of a number of samples are given in Table 4-2.

Table 4-2

sample	I	II	III	IV	V	VI	VII	VIII
$\kappa(0)$ (W/mK) T ≈ 300 K	3.80	2.80	2.35	6.0	4.75	4.70	6.25	7.5
$\kappa(0)$ (W/mK) T ≈ 90 K	2.80	1.90	2.10	2.3	1.80	- -	4.90	- -

The table shows that $\kappa(0)$ at room temperature roughly increases with increasing electron concentration, although there is considerable scatter in the magnitudes of $\kappa(0)$ of comparable samples (I, II, III and IV, V, VI). The thermal conductivity of Cd_3As_2 has been the subject of considerable attention in the literature. The value of 11 W/mK of a sample with $n \approx 3 \times 10^{24}$ m^{-3} first quoted by Turner et al.[17], seems far too high. This value has been measured by means of Harman's method[40], in which $\kappa(0)$ is deduced from the thermoelectric figure of merit $Z = \frac{\alpha^2(0)}{\rho(0)\kappa(0)}$. The value of $\alpha(0) = 140$ μV/K given by Turner, which is about twice that found by other authors, justifies the doubt about the value of 11 W/mK. Concerning the other values of $\kappa(0)$ reported in the literature, we would mention the papers by Spitzer et al.[6], Lovett and Ballentyne[22], Girandier[64], Goldsmid and Armitage[50].

Spitzer et al., who measured a large number of samples, found values of about 2.7 W/mK. These magnitudes were confirmed by the measurements of Goldsmid and Armitage, who used samples supplied by Spitzer. The values of $\kappa(0)$ reported in refs.22 and 64, however, are much higher and confirm our values of undoped material. Ballentyne and Lovett found $\kappa(0)$ to be about 4.8 W/mK for three samples with $n \approx 2 \times 10^{24}$ m^{-3}. A particularity

is that Armitage and Goldsmid established 5 W/mK for a sample supplied by Girandier.

In order to verify our results obtained with the absolute method described in chapter 2, we also carried out measurements on sample VI by two other methods. Using a modified Harman method† a value of 4.9 W/mK has been found for this sample. A second method, described by Schröder[65], yields 4.6 W/mK. So it may be concluded that the value obtained by the absolute method is correct.

Evidently, there seems to be a considerable difference between the structure and purities of the samples used by the various authors. Comparing the lattice and electronic contributions to $\kappa(0)$ of our samples with those of refs. 6 and 50, it appears that the discrepancies in the thermal conductivity are mainly due to the large deviations in the lattice contributions. The reasons for this disagreement is not clear; the suggestion that some of the samples have the high-temperature structure is unlikely, since this would result also in an even greater effect on the electron mobility. In addition, it should be mentioned that Spitzer et al. pointed out that there seems to be no relation between the electron mobility and the lattice thermal conductivity. Another unexplained feature is the behaviour of the thermal conductivity as a function of temperature in the range from liquid nitrogen to room temperature. As can be seen from Table 4-2 the thermal conductivity at liquid nitrogen temperature is even smaller than that at room temperature, whereas for purely lattice scattering we would expect κ_L to vary proportionally to T^{-1}. We will not discuss these anomalies in the thermal conductivities any further, since our attention is mainly directed to the change of κ with magnetic field, i.e. the electronic thermal conductivity. We believe that the above disagreements between the results reported for Cd_3As_2, can be solved only by a careful re-examination of these properties in single crystalline samples.

---

† *In this method the thermoelectric figure of merit has been obtained graphically from the difference between the voltages across the sample measured directly before and directly after a direct current sent through the sample is switched off : $V_{+o} - V_{-o} = V_{-o}$. ZT. In fact, the thermoelectric figure of merit is determined from the difference between the isothermal and the adiabatic resistivity of the sample (see ref. 66).*

4.3.2. Measurements of $\Delta\kappa^i(B)$

The variation of κ^i with increasing magnetic induction for a number of samples are given in Fig.4-18. The curves show the same tendency as the curves of the variations of $\Delta\alpha^i$ with magnetic induction in Figs. 4-5 and 4-6: the curvature becomes the more pronounced as the mobility is higher,

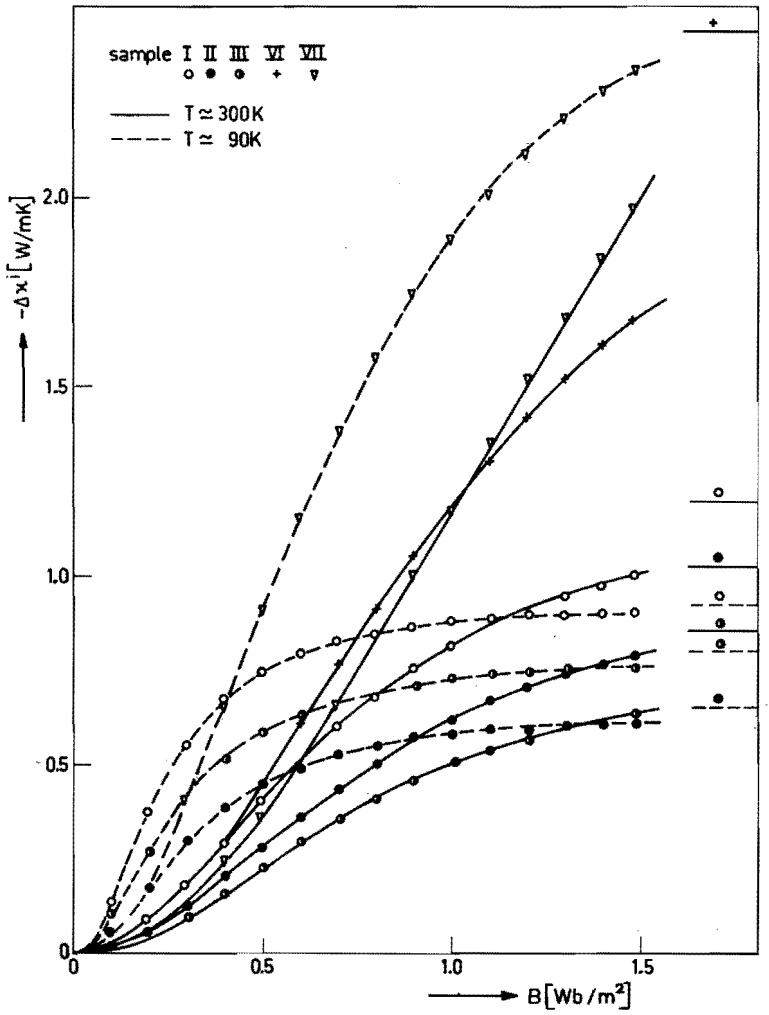

Fig. 4-18 Variations of the thermal conductivities with magnetic induction.

and at low temperatures almost complete saturation is reached for the samples I, II and III. The corresponding extrapolation graphs have been plotted in Fig.4-19.

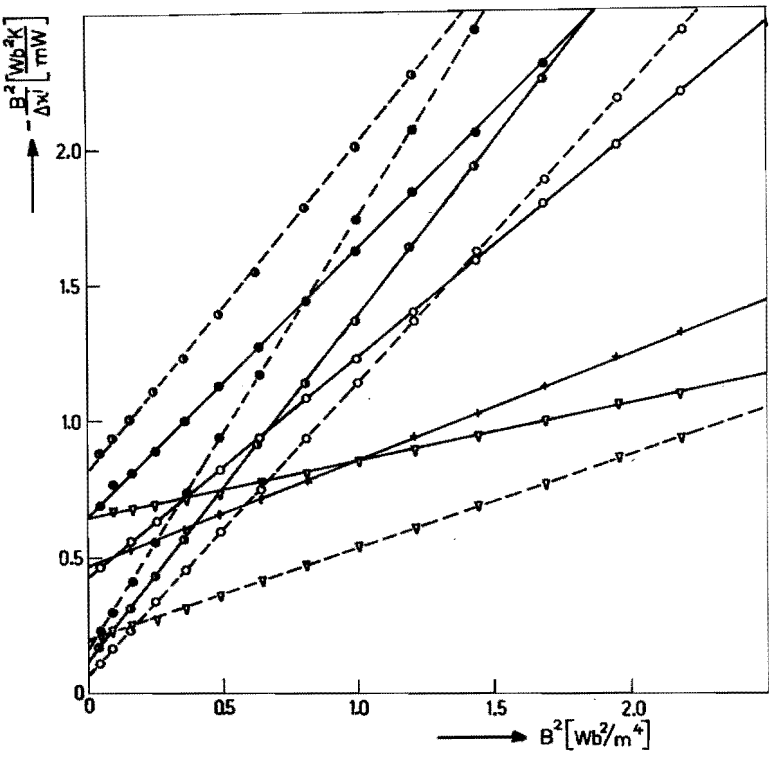

Fig. 4-19 Extrapolation graphs for the determination of $\kappa_E(0)$ *and* μ_T.

The measurements of the thermal conductivity have been carried out with a constant heat current density W_x and varying magnetic fields. The disadvantage of this method is that at each value of B, κ is determined from only one set of experimental values of W_x and ΔT_x, which enhances the possibility of errors. As a check, we also performed measurements on sample VII with constant magnetic induction and varying heat current densities. However, in this case the relation between W_x and the observed T_x is not linear ,since ΔT_x contains a component resulting from

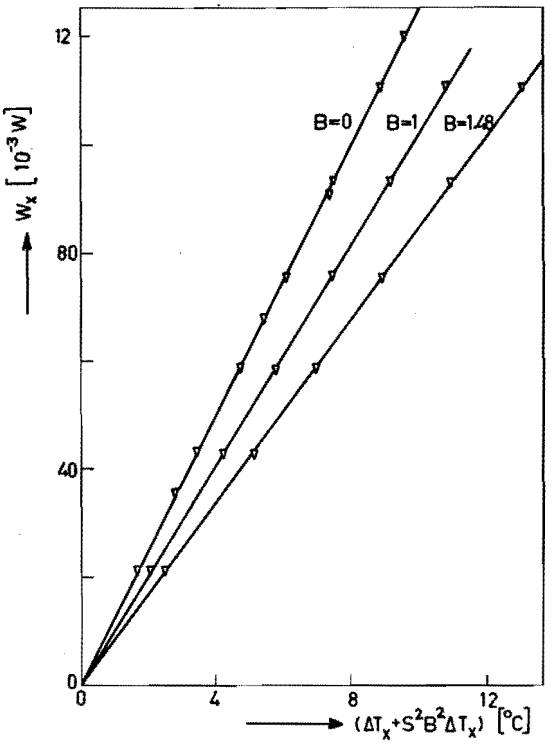

Fig. 4-20 Total heat current through sample VII versus corrected temperature difference at room temperature, for three values of the magnetic induction.

the Righi-Leduc effect acting on the Righi-Leduc effect ($-S^2B^2\Delta T_x$). See also eq. (2.3). Correcting each individual measurement for this effect results in the straight lines of Fig. 4-20. From the slopes of the lines we obtain values of κ^i equal to 6.22, 5.07 and 4.25 W/mK for B equal to 0, 1 and 1.48 Wb/m^2, respectively. These magnitudes are completely in agreement with those found from the procedure with a constant heat current density, viz. 6.25, 5.06 and 4.26 respectively.

From the slopes of the straight lines in Fig. 4-19 the values of $\Delta\kappa^i(\infty)$ can be determined. Assuming that the lattice component κ_L of the total thermal conductivity is unaffected by the magnetic field, the

saturation value $\Delta\kappa^i(\infty)$ is equal to the electronic thermal conductivity in zero-field $\kappa_E(0)$. Together with the resistivity at zero-field $\rho(0)$ and the average temperature T, the Lorenz number L can be determined from the Wiedemann-Franz law

$$\frac{\kappa_E(0).\rho(0)}{T} = L\,(\frac{k_o}{e})^2 \qquad (4.9)$$

If electric and thermal conductivity take place by a single type of charge carriers in a parabolic band, the theoretical Lorenz number L_o depends on the position of the Fermi level and on the scattering mechanism[67]. In non-degenerate semiconductors the Lorenz number is equal to about 2.0, 3.0 and 4.0 for scattering by acoustical phonons, optical phonons and ionised impurities, respectively. With increasing η the magnitude of L_o increases, and becomes equal to $\frac{\pi^2}{3}$ for infinite degeneracy ($\eta=\infty$), independent of the nature of the scattering mechanism. Since the dependence of the theoretical Lorenz number on the degree of degeneracy is only known for a parabolic band, we have to verify if this dependence also applies to carriers in a non-parabolic band. Therefore we have calculated the dependence of L_o on η for a Kane band and scattering by optical phonons. It appears that L_o decreases more rapidly with decreasing η than in the corresponding cases of a parabolic band : the value of $L_o/\frac{\pi^2}{3}$ is found to decrease from 0.98 to 0.89 with decreasing η from 16 to 4. With these results we are now able to determine the ratio L/L_o. As has been shown in section 3.4 we expect this ratio to be less than 1 if the scattering mechanism contains an inelastic contribution. Moreover, L/L_o must be equal to the ratio μ_T/μ_H, in which μ_T is the mobility determined from the thermomagnetic effects ($\Delta\alpha^i$,$\Delta\kappa^i$, S and N^i). The results and the discussion of the different values of L/L_o and μ_T/μ_H will be presented in section 4.5.

As in the case of the longitudinal Nernst effect (section 4.2.4), we are also able to compare the experimental and theoretical dependences of $\Delta\kappa/\kappa_E(0)$ and $\mu^2B^2/\Delta\kappa/\kappa_E$ on μB and μ^2B^2, respectively. These comparisons are shown in Figs. 4-21 and 4-22. We should mention, however, that the situation here is different from that in section 4.2.4. In fact, the experimental values of $\Delta\kappa/\kappa_E$ are determined with the assumption that the extrapolation formula (3.51) may be applied, which means that the "experimental" points for each sample must fit the same curve. Actually,

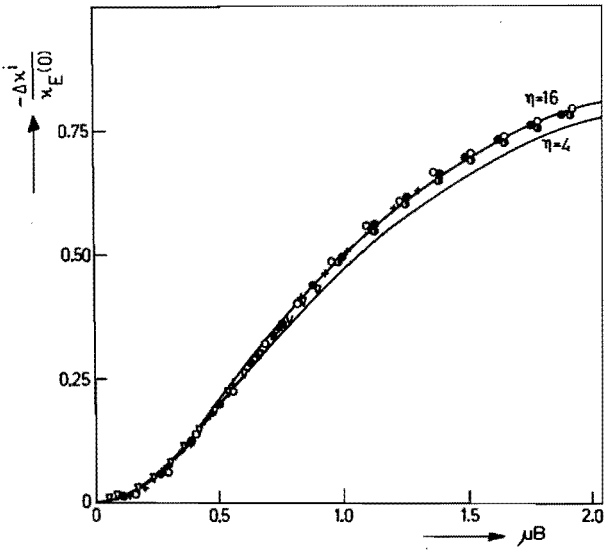

Fig. 4-21 Comparison of theoretical and "experimental" relative changes of the electronic thermal conductivities, at room temperatures.

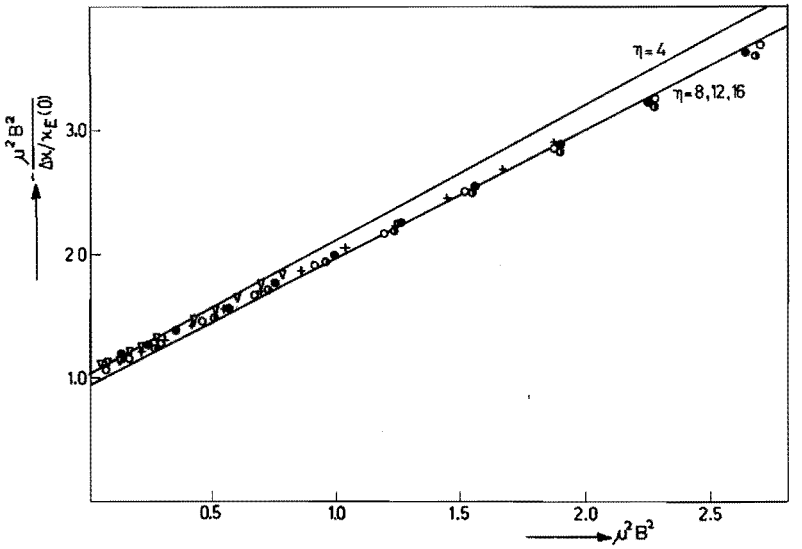

Fig. 4-22 Comparison of theoretical and "experimental" extrapolation graphs.

Figs.4-21 and 4-22 only show that the simple extrapolation formula is valid for a Kane-type conduction band, if the thermal mobility is used instead of the Hall mobility (see further section 4.5).

4.4. Righi-Leduc and Nernst effects

4.4.1. Measurements of the Righi-Leduc coefficient

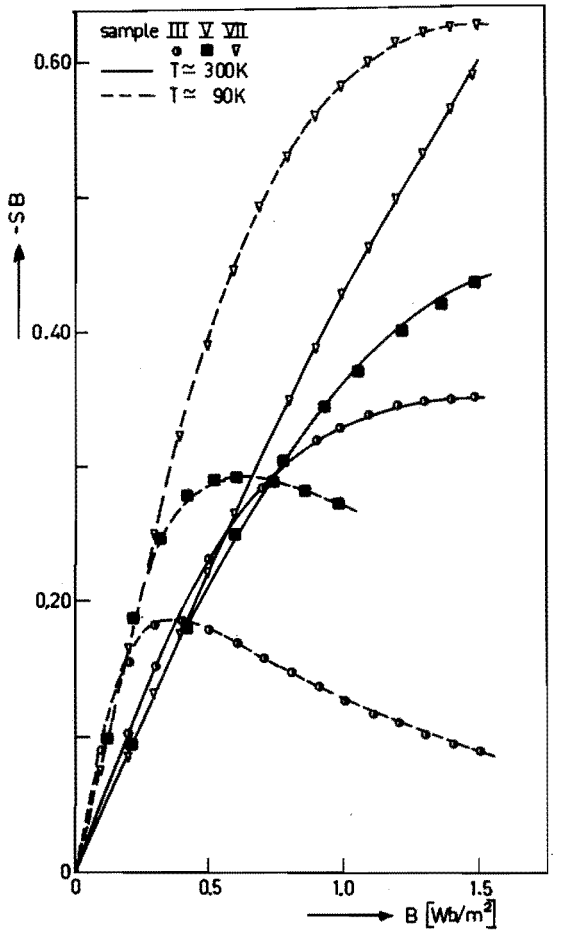

Fig. 4-23 Righi-Leduc coefficients vs. magnetic induction.

Apart from the fact the Righi-Leduc coefficient should be measured in order to convert the adiabatic into the isothermal transport coefficients (see eqs. (2.1) to (2.3)), SB can give valuable additional information on the transport mechanism. Considering Fig.4-23, in which for three samples SB has been plotted vs. B at room temperature as well as at liquid nitrogen temperature, we mention the following features.

First, it appears that the Righi-Leduc coefficient is negative, which is in agreement with the fact that the sign of SB is determined by the sign of the charge carriers. The Righi-Leduc effect is the thermal analogue of the Hall effect, for which reason it is often called the thermal Hall effect.

Secondly, the values of SB (continuing the analogy to the Hall effect, this quantity might be called the thermal Hall angle) are particularly large in Cd_3As_2. A value of SB = 0.60 at B = 1.5 Wb/m^2 means that, with a temperature gradient of about $10^oC/cm$ and a dimension of the sample in the y-direction of 5 mm (typical values of sample VII), the temperature difference in the y-direction is as high as 3^oC. This large magnitude is due to the high mobility, the high electron concentration and the relatively low lattice thermal conductivity (eq. (3.52)).

Further inspection of Fig.4-23 shows that the room temperature curves of the samples III and V tend to reach maximum values, which is still more pronounced at low temperatures. It can be proved from eq. (3.52) that the maximum of SB, and the value of B at which this maximum occurs, are given by

$$(SB)_{max} = \frac{1}{2} \frac{\kappa_E(0)}{\kappa_L} \sqrt{1 + \frac{\kappa_E(0)}{\kappa_L}} \quad \text{at } B = \frac{1}{\mu} \sqrt{1 + \frac{\kappa_E(0)}{\kappa_L}}$$

The values of $\frac{\kappa_E(0)}{\kappa_L}$ and μ of the samples III, V and VII increase and decrease, respectively in this sequence, so that the observed locations and heights of the maxima are qualitatively in agreement with theory. However, using these characteristics of the maxima for the determination of μ_T would be very inaccurate, so that for this purpose we used another method, viz. by plotting $\frac{1}{S}$ vs. B^2. See Fig.4-24. Note that the vertical axis on the left-hand and the right-hand side of this figure refer to the values of $\frac{1}{S}$ at room temperature and at liquid nitrogen temperature, respectively. The values of μ_T are given in section 4.5 together with other numerical results of the samples.

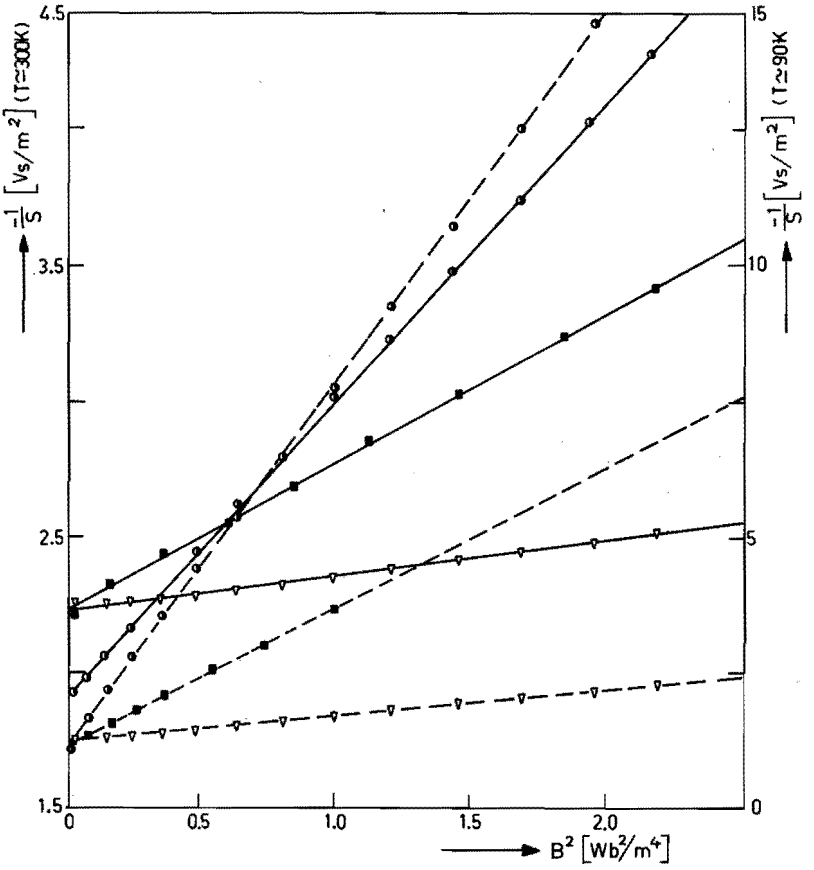

Fig. 4-24 Extrapolation graphs .

The comparison with the theoretical predictions from Harman's theory is more complicated in this case, since the Righi-Leduc coefficient is not only dependent on the band and scattering parameters but also on the lattice thermal conductivity. The average value of κ_L of the samples III, V and VI is about 2 W/mK, so we used this value in the calculations. See Fig. 4-25. The agreement between theory and experiment is satisfactory.

It is well worth while investigating the Righi-Leduc effect further, particularly in samples with very strong degeneracy, because of the fact that this study gives important information on the numerical value of the

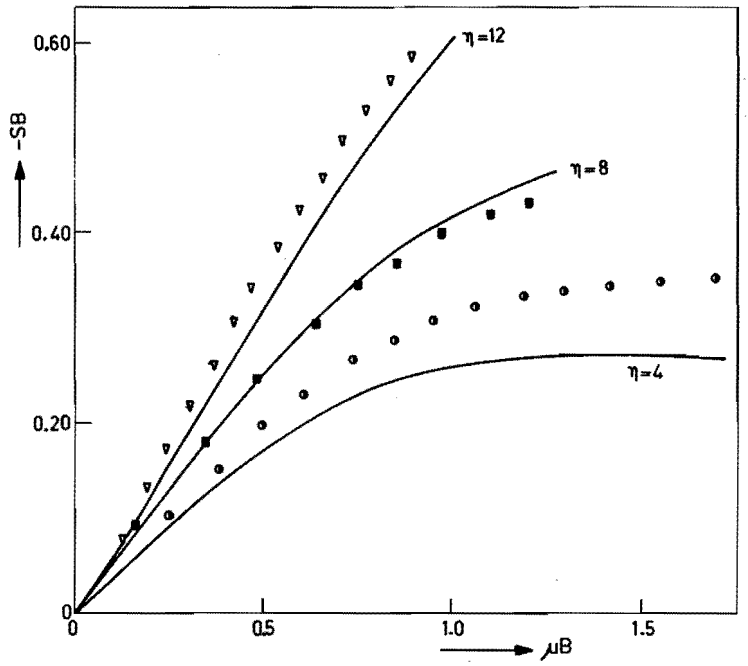

Fig. 4-25 Comparison of theoretical and experimental values of the Righi-Leduc coefficients. For the theoretical curves a value of κ_L = 2 W/mK *has been used.*

band gap of Cd_3As_2. As can be seen from Fig. 4-25 there are important differences in the magnitudes of SB at constant values of μB and κ_L. This behaviour is greatly different in case a parabolic conduction band applies. For a parabolic conduction band and acoustical lattice scattering the curves of SB vs. μB with constant κ_L nearly completely coincide with a reduced Fermi level between 8 and 12, whereas for a Kane band and optical lattice scattering the curves diverge the more as η becomes larger. In the region of large values of η, the Righi-Leduc effect is also very sensitive to the reduced band gap x_g. These properties offer the possibility of determining the band gap more accurately than from the other thermomagnetic effects. Sample VII was chosen for the purpose, since it is one of our most extensively investigated samples. From Fig. 4-14 it appears that it would

have a reduced Fermi level of 12, if it is assumed that $x_g = 6$. The thermal conductivity of the sample was determined to be 6.22 W/mK, consisting of lattice and electronic components of 1.65 and 4.57 W/mK, respectively. The mobility determined from the Hall effect, Seebeck effect, thermal conductivity, Righi-Leduc effect and Nernst effect was found to be 0.60 $m^2/V.s$ with a scatter less than 0.03. Using κ_L = 1.65 W/mK and η = 12 we calculated the Righi-Leduc coefficients vs. μB for x_g = 4,5,6,7. (Fig.4-26). The experimental points for sample VII lie between the curves for x_g = 5 and 6, so we may conclude that the value of x_g = 6 obtained from Fig.4-9 is confirmed by this sensitive check.

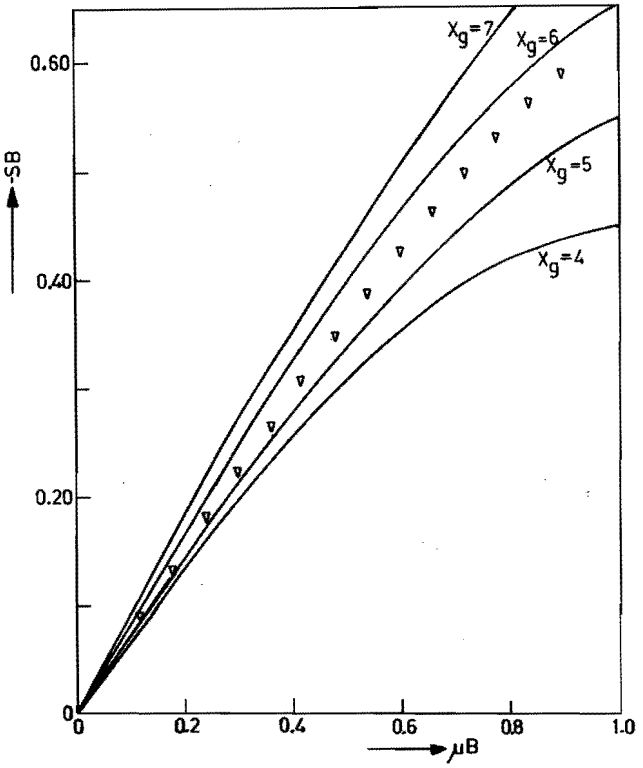

Fig.4-26 A detailed comparison of the experimental values of SB for sample VII with theoretical predictions for η = 12, κ_L = 1.65 W/mK and four values of x_g.

4.4.2. Measurements of the transverse Nernst coefficient

As has been mentioned in section 2.3 the isothermal transverse Nernst coefficients in Cd_3As_2 are hard to determine accurately. At room temperature, maximum values of N^iB are about 8 μV/K, whereas at low temperatures these maxima are about a factor 4 smaller. See Fig.4-27. Notwithstanding the

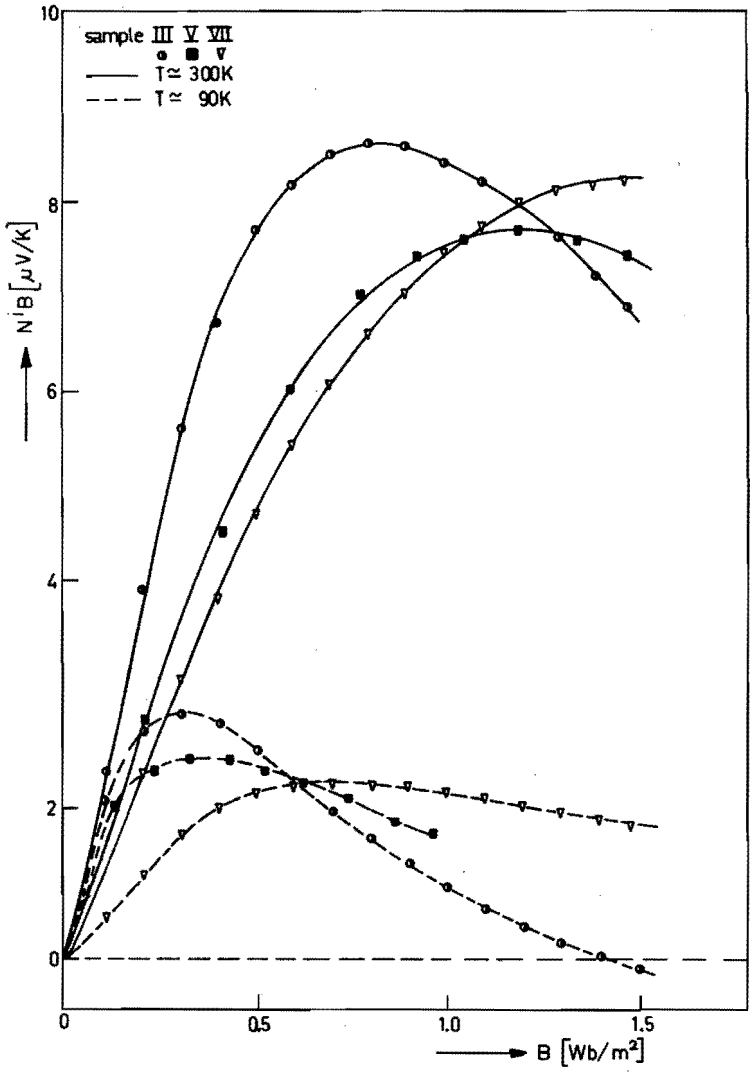

Fig.4-27 Isothermal transverse Nernst coefficients vs. magnetic induction.

smallness, we can use the sign and the slopes of the curves at B = 0 to check the results obtained from the other thermomagnetic effects. From eq. (3.47)

$$N^i(0) = \frac{-2}{3}\,\mu\,|\alpha^i(\infty)|\,\{r-3\gamma-\frac{1}{2}\}$$

it can be seen that the sign of the Nernst effect is independent of the sign of the charge carriers, but only depends on the sign of the form $(r-3\gamma-\frac{1}{2})$. If we substitute $\gamma \simeq 0.30$, it appears that a positive Nernst effect implies that r must be less than about 1.5, thus including the possibility of optical phonon scattering (r=1). A different situation occurs if a parabolic band applies, as in that case $\gamma = 0$ and a positive Nernst effect is related to the conduction that $r < 0.5$. As an illustration, we draw

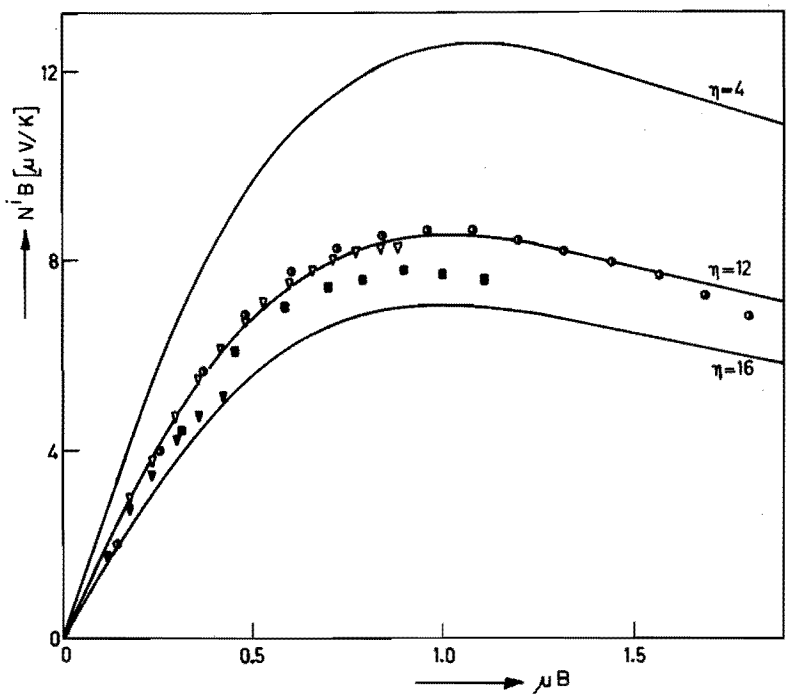

Fig. 4-28 Comparison of theoretical and experimental values of the transverse Nernst coefficients.

attention to the fact that the Nernst effect completely vanishes if the charge carriers in a parabolic band are scattered by neutral impurities ($r = \frac{1}{2}$).

Inspection of eq. (3.47) also shows that the slopes of the curves at B = 0 should increase with increasing $\mu\alpha^i(\infty)$, which is confirmed by the experimental curves in Fig.4-27. For the locations and the heights of the maxima the following results can be derived

$$(N^iB)_{max} = \frac{1}{2} \left|\Delta\alpha^i(\infty)\right| \qquad \text{at } B = \frac{1}{\mu}$$

From the room temperature values of $\Delta\alpha^i(\infty)$ indicated in Fig.4-5, the maxima of the curves for the samples III, V and VII should be about 12, 11 and 9 μV/K, respectively. Taking into account the inaccuracies in the measurements of N^iB, the agreement is satisfactory. The same conclusion holds regarding the comparison of theory and experiment given in Fig.4-28.

According to eq. (3.53) graphs of $1/N^i$ vs.B^2 should give straight lines from which values of $\Delta\alpha^i(\infty)$ and μ_T would be obtained. However, because of the inaccuracies in N^iB and the fact that the Nernst effect is also particularly sensitive to sample inhomogeneities[68], for most of the samples it is not possible to give more than an estimate of μ_T (see section 4.5).

Finally, Fig.4-29 contains graphs of the experimental values of $\frac{\Delta\alpha^i(B)}{N^iB}$ against B for sample VII at room temperature and at liquid nitrogen temperature. From eqs. (3.49) and (3.53) one may verify that

$$-\frac{\Delta\alpha^i(B)}{N^iB} = \mu B$$

so that the points in Fig.4-29 should be on straight lines with slopes equal to μ (300 K) and μ (90 K), respectively. These lines are drawn in the figure. Because of the inaccuracies in $\Delta\alpha^i(B)$, and particularly in N^iB, one may hardly expect the experimental points to fit these lines. Nevertheless, the deviations at room temperature are only very small. At liquid nitrogen temperature the discrepancies are much larger and increase with increasing magnetic field. Moreover, the Nernst coefficients of the samples I, II and III at low temperatures, of which one representative curve is shown in Fig.4-27, even become negative at high magnetic fields.

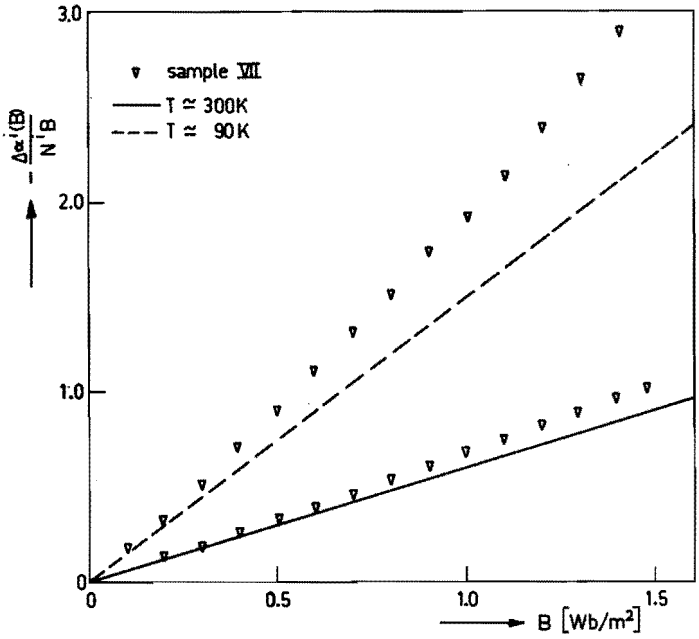

Fig. 4-29 A plot of $\frac{\Delta\alpha^i(B)}{N^i B}$ *vs. magnetic induction for sample VII, showing the deviations from the expected lines.*

4.5. Inelastic contribution to the scattering mechanism

In Table 4-3 the data are given of the room temperature mobilities determined from the different thermomagnetic effects, compared with the Hall mobilities. The symbols $\mu_T(\Delta\alpha)$, $\mu_T(\Delta\kappa)$ and $\mu_T(S)$ refer to the thermal mobilities obtained from the extrapolation graphs for the longitudinal Nernst effect (Fig.4-7), the Maggi-Righi-Leduc effect (Fig.4-19) and the Righi-Leduc effect (Fig.4-24), respectively. The mobilities $\mu_T(N)$, determined from the Nernst effect, are inaccurate, and therefore are not taken into account in the average thermal mobility $\overline{\mu}_T$. In the last two rows of the table, the values of L/L_o (obtained from Fig.4-19 together

with the theoretical calculations of L_o for a Kane band with optical phonon scattering) are compared with the values of $\bar{\mu}_T/\mu_H$

Table 4-3

sample	I	II	III	IV	V	VI	VII	VIII†
μ_H (m/Vs)	1.60	1.44	1.49	0.90	0.78	1.02	0.60	0.30 ± 0.05
$\mu_T(\Delta\alpha)$	1.23	1.20	1.20	0.93	0.79	1.06	0.60	0.3 ± 0.1
$\mu_T(\Delta\kappa)$	1.35	1.24	1.22	0.87	0.82	0.93	0.59	0.4 ± 0.1
$\mu_T(S)$	1.13	1.05	1.08	0.88	0.80	0.90	0.58	0.3 ± 0.1
$\mu_T(N)$	1.4 (± 0.1)	1.35 (± 0.1)	1.25 (±0.1)	1.0 (±0.2)	1.0 (±0.2)	-	0.62 (±0.05)	-
$\bar{\mu}_T/\mu_H$	0.77	0.80	0.78	0.99	1.03	0.96	0.98	-
L/L_o	0.93	0.75	0.72	1.03	1.02	0.94	1.01	1.0 ± 0.1

† *The results for sample VIII are very inaccurate, owing to the reasons mentioned in section 4.1.*

As can be seen in the table, the magnitudes of the ratios $\bar{\mu}_T/\mu_H$ and L/L_o are in surprisingly good agreement with each other. It must be concluded that the inelastic contribution to the scattering mechanism in the samples III to VII is negligible, whereas for the samples with lowest electron concentrations (I, II and III) a considerable inelastic contribution is present. This partially inelastic scattering has been taken into account in the graphs of the comparisons of experimental results with theoretical predictions : for the samples I, II and III the average values of μ_T have been substituted for the experimental mobility, whereas for the other samples it does not matter which of the two mobilities, $\bar{\mu}_T$ or μ_H, is used. That the thermal mobility should be used, in case of partially inelastic scattering, can be demonstrated most clearly with the help of Fig.4-21. The theoretical curves virtually coincide for all values of the reduced Fermi levels; a consequence of the use of the method by which $\Delta\kappa/\kappa_E(0)$ has been determined, is that the experimental points must

fit these curves. This requirement is only met when the thermal mobilities are used for the samples I, II and III.

Evidently, the partially inelastic scattering only occurs in the samples with lowest electron concentrations. Armitage and Goldsmid[50], who studied extensively the problem of inelastic scattering in Cd_3As_2 samples with electron concentrations in the range of 1 to 2.5 × 10^{24} m^{-3}, also found an increasing inelastic contribution with decreasing electron concentration. This fact has not yet been explained, since, if the scattering is due to interaction with optical phonons, the degree of inelasticity should be independent of the electron concentration.

According to the theory of Korenblit and Sherstobitov the inelastic contribution should become greater as the temperature falls. Inspection of Table 4-4 shows that the ratios L/L_o at liquid nitrogen temperature are indeed lower than those at room temperature, particularly for the samples IV, V and VII. However, the values of μ_T/μ_H exhibit a wide spread and do not fit the values of L/L_o; in some case μ_T/μ_H even becomes greater than unity.

Table 4-4

sample	I	II	III	IV	V	VII
L/L_o	0.80	0.62	0.74	0.55	0.60	0.90
μ_T/μ_H	0.6-0.8	0.6-0.9	0.5-0.8	0.6-1.1	0.8-1.2	0.88

We do not have an explanation of these contradictory results. The possibility that the scattering at low temperature is only due to impurities and lattice imperfections, seems to be ruled out by the fact that these types of scattering are elastic, so that the ratio L/L_o must be equal to 1. A similar strange behaviour has been observed from the measurements of the thermal conductivity (see section 4.3). The lattice thermal conductivity at liquid nitrogen temperature is smaller than at room temperature, which would indicate scattering by ionised impurities. However, the Hall mobilities of the different samples at liquid nitrogen temperature are about a factor 2.5 greater than their room temperature values, which supports the idea that the samples are rather pure. Remembering the

positive sign of the initial slopes of the low temperature curves N^iB vs.B (Fig.4-27), this fact also gives strong evidence that scattering completely dominated by ionised impurities should be excluded (r equals 2 for this scattering mechanism, which would result in a negative Nernst coefficient at vanishing magnetic field).

Summarising we may conclude that in our samples the scattering mechanism of the electrons at liquid nitrogen temperature is very complicated. Probably, a number of competitive mechanisms are present, of which those leading to a partially inelastic scattering are more important than others. In this connection it is worth noting another source of inelastic scattering which seems to be important in degenerate semiconductors with a partially ionic character, viz. electron-electron interactions[49]. The low values of the experimental Lorenz numbers in PbTe, PbSe and other chalcogenides have been attributed to electron-electron scattering. L/L_o in these compounds varied between 0.5 and 1.0, depending on temperature and electron concentration. Carrier-carrier collisions which produce a redistribution of carrier energy, can produce a considerable change in the thermal flux and so influence thermomagnetic effects noticeably more than electrical transport effects, thus leading to thermal mobilities lower than the Hall mobility. If collisions between conduction electrons also played an important part in Cd_3As_2 at low temperatures, the particularities observed in our samples would become more explicable.

CHAPTER 5

SUMMARISING REMARKS AND CONCLUSIONS

In this chapter we will review and comment upon the results obtained from our measurements of the thermomagnetic effects.

The most important argument upon which the analyses are based, is the fact that it is possible to determine the electron effective mass at the Fermi level from the measurements of the electron density and the saturation value of the Seebeck coefficient, without knowing the scattering mechanism. The conditions under which this procedure of determining m^* is permissible, are strong degeneracy of the electron gas and symmetry of the energy surfaces with respect to the wave vector. The temperature dependences of the Seebeck coefficient, resistivity, and Hall coefficient (Figs.4-1, 4-2 and 4-3) prove the validity of the first condition in Cd_3As_2. The measurements of the magneto-resistance effect and of the Shubnikov- de Haas effect in oriented single crystals, reported in the literature[15,27], strongly evidence a nearly spherically symmetric conduction band centered at the origin of k-space.

The dependence of the electron effective mass on electron concentration in the range of about 0.7 to 13 $\times$ 10^{24} m^{-3} has been determined, and was found to be consistent with the relation between these properties expected for a Kane conduction band model. The experimental points in Fig.4-9 fit so well a straight line that we conclude that the reported value of $P = 8.1 \times 10^{-8}$ eVcm (determined from the slope of the line) is very accurate. This magnitude of P is moreover confirmed by the low temperature results given in Fig.4-10. The point of intersection of the line with the vertical axis in Fig.4-9 lies so close to the origin that the band gap E_g cannot be obtained with such a high accuracy. Comparisons of the experimental results with theoretical predictions, particularly those of the Righi-Leduc effect in sample VII, however, show that the choice of $E_g = 0.15$ eV is justifiable.

The assumption of a Kane type conduction band with the above mentioned numerical values of the parameters P and E_g, completely determines the relation between the electron concentration and the Fermi level. For the samples investigated by us the reduced Fermi levels were found to range from 4 to 16 at room temperature. This means that, dependent on electron concentration the Fermi level ε_F lies between 0.10 and 0.40 eV above the bottom of the conduction band. With these magnitudes of ε_F in mind, we will compare the value of E_g with those reported in the literature for Cd_3As_2.

As has already been mentioned in Chapter 1, the energy gaps quoted by several authors show great differences. Before discussing these discrepancies in respect of our results, we would first consider the physical meaning of the symbol E_g. In eq. (3.29), E_g is the energy separation between the top of the light hole (valence) band and the bottom of the light electron (conduction) band at k = 0. In InSb the maximum of the light hole band and the minimum of the light electron band are at Γ_8 and Γ_6, respectively, while, moreover, there exists a heavy hole band degenerated with the light hole band at Γ_8. In this case the direct gap between light hole and light electron band $E_g = \Gamma_6 - \Gamma_8$ is positive (The symmetry points are labelled with the appropriate double group representation for the zincblende space group). In the compounds HgTe and HgSe, however, an inverted energy ordening scheme occurs[55] : $\Gamma_8 > \Gamma_6$. The Γ_6 light electron band of InSb has become the light hole band of HgTe and HgSe, whereas the light hole Γ_8 and heavy hole Γ_8 band has become the Γ_8 light electron band and a heavy hole like Γ_8 band, respectively. The direct energy gap between the light hole and light electron band $E_g = \Gamma_6 - \Gamma_8$ is negative in this case. It should be noted that the direct gap E_g need not be the same as the thermal band gap E_t. In InSb the $\Gamma_6 - \Gamma_8$ separation is also the thermal gap, but in the inverted structures the thermal gap is zero, owing to the fact that the degeneracy point at Γ_8 is both the top of the heavy hole and the bottom of the light electron band. It has been shown that the heavy hole band maximum is shifted from $k = 0$ and is bent upwards by several hundredths of an electronvolt, so that the thermal band gap is even negative (semimetal with overlapping bands). In HgTe, E_g and E_t are reported to be about -0.30 and -0.02 eV, respectively.

From the above exposition about the difference between E_g and E_t it becomes clear that in our case we determined the value of the direct gap between the light hole and light electron band. However, from Fig.4-9 it

is impossible to deduce the sign of E_g, since eq. (3.29) upon which the analysis is based, only contains a term proportional to $|E_g|$. On account of this result it is impossible to decide whether Cd_3As_2 would have an InSb-like or an inverted band structure.

Although we do not agree with the numerical values of P and E_g reported by Wagner et al[33a], their measurements give strong evidence of an inverted band structure. Assuming that their proposal of this structure does indeed apply to Cd_3As_2, the quoted discrepancies between the values of the band gap can be explained to a certain extent. The literature values of the band gap are clearly centred around two definite magnitudes, viz. 0.15 and 0.60 eV respectively. From the temperature dependences of the resistivity and the Hall coefficient of samples with electron concentrations of about $1\text{-}2 \times 10^{24}$ m^{-3}, the energy gaps are found to vary from 0.13 to 0.20 eV. Zdanowicz[14] and Turner et al.[17] observed weak absorption edges at 0.13 and 0.14 eV, respectively, whereas strong edges were found at about 0.60 eV[13,14]. Taking into account that these measurements are all concerned with samples of $n \approx 2 \times 10^{24}$ m^{-3} and that the Fermi levels in such samples lie about 0.15 - 0.20 eV above the bottom of the conduction band, the low energy gap might be due to indirect transitions from the heavy hole band to the light electron band shifted from 0 eV due to the large Burnstein effect[67]. Haidemenakis et al.[26] studied high-field interband magneto-absorption in a Cd_3As_2-sample with $n = 2 \times 10^{24}$ m^{-3} and found that the interband oscillations disappeared for photon energies below about 0.13 eV. By straight line extrapolation they found an energy gap of 0.025 eV between a light electron band and a heavy hole band. The Burnstein shift would then be about 0.13 eV, somewhat lower than we would expect from the calculation of the Fermi level for a sample with $n = 2 \times 10^{24}$ m^{-3} (viz. 0.20 eV, see Fig.4-14), which might be explained as a heavy hole band overlapping the light electron band.

The second absorption edge of about 0.60 eV could originate from direct transitions between the light hole and the light electron band, taking into account the Burnstein shift. In the Kane model these two bands have the same $\varepsilon(k)$ relation, so the Burnstein shift would be twice the Fermi-level, which leads to an energy distance of $E_g + 2\,\varepsilon_F = 0.55$ eV for a sample with $n = 2 \times 10^{24}$ m^{-3}. Using $E_g = 0.38$ eV and $\varepsilon_F = 0.15$ eV, Wagner et al. reported 0.68 eV for the quantity $E_g + 2\,\varepsilon_F$, which is also in good agreement with the observed absorption edge. However, we believe that this value has

the reported magnitude more or less accidentally. First, a value of $E_g = 0.38$ seems far too high. For, from their values of E_g and P results an effective mass at the bottom of the conduction band of $m^*(0) = 0.025\ m_o$, which is only slightly smaller than the value of $m^* = 0.032\ m_o$ found in our samples with a Fermi-level of 0.10 eV. Secondly, a Fermi level of 0.15 eV is too low for a sample with $n = 2 \times 10^{24}\ m^{-3}$.

As a final remark we would observe that the above suggestions that cadmium arsenide should have an inverted band structure, or might even be considered to have a band overlap, are only speculative. It would be wrong to assume that our work leads definitely to the solution of all problems concerning the complexity of the band structure of this compound. There are, however, two other phenomena, viz. the magneto-resistance and the transverse Nernst effect, which also indicate that the transport properties cannot be fully described by only one type of charge carriers in a non-parabolic band. Although the interpretation of the measurements of both effects are hindered if inhomogeneities are present in the samples[68,69], yet the anomalous behaviour of these effects seems too systematic to lead to the impression that it should be completely attributed to physical imperfections. We calculated the magneto-resistance for a Kane band model with optical phonon scattering as a function of μB and different values of η. As may be expected, the magneto-resistance is very small if only one type of carriers takes part in the conduction mechanism : $\frac{\Delta\rho}{\rho(0)}$ at $\mu B = 1$ lies between 5×10^{-3} and 5×10^{-2} for $4 < \eta < 16$ (room temperature). The experimentally observed values of $\frac{\Delta\rho}{\rho(0)}$ at the same μB are about a factor 10 greater. The transverse Nernst effects at low temperatures in samples I, II and III become negative at high values of B (see Fig.4-27). Although in section 4.5 we pointed out that the scattering at low temperatures is very complicated, a change of the sign of the Nernst coefficient with increasing B cannot occur for one type of charge carriers, whatever the scattering mechanism may be. Both features might be due to the presence of holes in a heavy hole band near the bottom of the conduction band.

Since the band parameters E_g and P have been determined independently of the scattering mechanism, the signs and field-dependences of the thermomagnetic transport coefficients may be used to obtain the scattering parameter r. These analyses have been most extensively carried out from the measurements of the Seebeck coefficient. Figs. 4-12, 4-15 and 4-17 show

clearly that at room temperature the dominant scattering of the electrons is due to interactions with polar optical phonons. This conclusion is also confirmed by the magnetic field dependences of the Righi-Leduc coefficient (Figs.4-25 and 4-26), and to a lesser extent by the Nernst effect (Fig.4-28).

The scattering mechanism at liquid nitrogen temperature in our samples is so complicated that we would not hazard a quantitative explanation of the field dependences of the thermomagnetic coefficients with a Kane band model and optical phonon scattering only. Under the assumption that P and E_g are equal to those at room temperature (it is impossible to obtain a value of E_g at low temperatures from Fig.4-10), we have calculated the thermomagnetic transport coefficients as functions of μB with the appropriate values of n. It appeared that the experimental results for some of the effects are qualitatively rather well in agreement with the theoretical curves for $r = 1$. As has been mentioned earlier, this value of r probably will be an average for a number of mechanisms.

The theory of Harman and Honig, upon which our numerical calculations have been based, is only applicable if the scattering mechanism is elastic, i.e. in case of scattering by optical phonons the measuring temperature should be sufficiently far above the characteristic temperature for longitudinal optical phonons Θ_L. That the Debije temperature Θ_o, determined from the specific heat measurements, equals 164 K, does not mean that we now also know exactly the value of Θ_L. It is likely that the Debije temperature for the longitudinal optical phonons is higher than Θ_o; in InSb, Θ_o and Θ_L are reported to be 206 and about 290 K, respectively. However, our major aim, viz. to know the order of magnitude of Θ_L, has been achieved. A confirmation that Θ_L is low, has been given by the fact that the thermal and the Hall mobilities at room temperature are nearly equal. The conclusion that the scattering in Cd_3As_2 at room temperature is caused by polar optical phonons, bears out once more that this type of scattering is more important than has been assumed earlier in the literature, particularly in semiconductors with non-parabolic conduction bands. For example, the dominant scattering mechanism at room temperature in n-type InSb, HgTe and HgSe is also caused by interaction with optical phonons[57].

Reviewing once more the most important results obtained from our thermomagnetic measurements on cadmium arsenide, apart from the speculative

suggestions about band structure details, and scattering mechanism at low temperatures, we come to the following conclusions.

The theory of Harman and Honig is particularly useful for analysing the magnetic field dependences of the thermomagnetic transport coefficients of degenerate n-type semiconductors with a Kane type conduction band. On the other hand, the Polish variant of the theory is more valuable for the interpretation of the thermomagnetic coefficients in the limits of vanishing and very strong magnetic fields.

The concentration dependence of the electron effective mass can be quantitatively well explained by a Kane type conduction band; there is no need of such a two-band model as proposed by Sexer to understand this dependence.

The room temperature values of the parameters of Kane's model applied to cadmium arsenide are found to be $P = 8.1 \times 10^{-8}$ eVcm, $E_g = 0.15$ eV and $m^*(0) = 0.012\ m_o$.

The dominant scattering mechanism at room temperature is caused by interaction of electrons with polar optical phonons. At liquid nitrogen temperature, a number of scattering mechanisms are simultaneously active, probably because of the imperfection of our samples.

REFERENCES

1. S.F. Zemczuzny, Intern. Z. Metallog., 4, 228 (1913).
2. M. Hansen, Constitution of Binary Alloys, McGraw-Hill, New York, (1958).
3. G.A. Silvey, V.J. Lyons, V.J. Silvestri, J. Electrochem. Soc., 108, 653 (1961).
4. G.A. Castellion, L.C. Beegle, J. Phys. Chem. Sol., 26, 767 (1965).
5. D.R. Lovett, D.W.G. Ballentyne, Brit. J. Appl. Phys., 18, 1399 (1967).
6. D.P. Spitzer, G.A. Castellion, G. Haacke, J. Appl. Phys., 37, 3795 (1966).
7. B. Koltirine, M. Chaumereuil, Phys. Stat. Sol., 13, K1 (1966).
8. H. Matsunami, private communication.
9. G.A. Steigman, J. Goodyear, Acta Cryst., B24, 1062 (1968).
10. A. Jayaraman, T.R. Anantharaman, W. Klement, J. Phys. Chem. Sol., 27, 1605 (1966).
11. N. Sexer, J. Phys. Radium, 22, 807 (1961).
12. A.J. Rosenberg, T.C. Harman, J. Appl. Phys., 30, 1621 (1959).
13. T. Moss, Proc. Phys. Soc. (London), 63, 167 (1950).
14. L. Zdanowicz, Phys. Stat. Sol., 20, 473 (1967).
15. W. Zdanowicz, Acta Phys. Pol., 21, 541 (1962).
16. N. Sexer, Phys. Stat. Sol., 14,K43 (1966).
17. W.J. Turner, A.S. Fischler, W.E. Reese, Phys. Rev., 121, 759 (1961).
18. W. Zdanowicz, Acta Phys. Pol., 20, 647 (1961).
19. N. Sexer, C.R. Acad. Sc. (Paris), 259, 1081 (1964).
20. E.O. Kane, J. Phys. Chem. Sol., 1, 249 (1956).
21. N. Sexer, Phys. Stat. Sol., 21, 225 (1967).
22. D.W.G. Ballentyne, D.R. Lovett, J. Phys. D (Solid State Phys.), 1, 585 (1967).
23. D.W.G. Ballentyne, private communication.
24. V.Y. Shevchenko, G.I. Goncharenko, V.F. Dvoryankin, F.M. Gashimzade, Sov. Phys.-Semicond., 3, 771 (1969).
25. D.R. Lovett, Phys. Lett., 30A, 90 (1969).
26. E.D. Haidemenakis, M. Balkanski, E.D. Palik, J. Tavernier, Proc. Int. Conf. Phys. of Semicond., Kyoto, 189 (1966).
27. I. Rosenman, Proc. Int. Conf. Phys. of Semicond., Kyoto, 370 (1966).

28. D. Armitage, H.J. Goldsmid, Phys. Lett., 28A, 149 (1968).
29. I. Rosenman, J. Phys. Chem. Sol., 30, 1385 (1969).
30. F.A.P. Blom, J.Th. Schrama, Phys. Lett., 30A, 245 (1969).
31. N.A. Goryunova, V.M. Muzhdaba, M. Serginov, S.S. Shalyt, Sov. Phys.-Solid State, 11, 225 (1969).
32. F.A.P. Blom, A. Huyser, Solid State Comm., 7, 1299 (1969).
33a. R.J. Wagner, E.D. Palik, E.M. Swiggard, Phys. Lett., 30A, 175 (1969).
33b. P.J. Lin-Chung, Phys. Rev., 188, 1272 (1969).
34. A.B.D. v.d. Meer, afstudeerverslag THE (1970) (In Dutch).
35. A.J. Strauss, A.J. Rosenberg, J. Phys. Chem. Sol., 17, 278 (1961).
36. I. Isenberg, B.R. Russel, R.F. Greene, Rev. Sci. Instr., 19, 686 (1948).
37. J. Volger, Phys. Rev. 79, 1023 (1950).
38. J.R. Drabble, R. Wolfe, J. Electron, 3, 259 (1957).
39. H.J. Lippman, F. Kuhrt, Z. Naturforsch., 13a, 462, 474 (1958).
40. R. Simon, R.T. Bate, E.H. Lougher, J. Appl. Phys., 31, 2160 (1960).
R. Simon, J.H. Cahn, J.C. Bell, J. Appl. Phys., 32, 46 (1961).
41. T.C. Harman, J.M. Honig, J. Phys. Chem. Sol., 23, 913 (1962).
42. T.C. Harman, J.M. Honig, B.M. Tarmy, J. Phys. Chem. Sol., 24, 835 (1963).
43. J. Kolodziejczak, Acta Phys. Polon., 20, 289, 379 (1961).
J. Kolodziejczak, L. Sosnowski, Acta Phys. Polon., 21, 399 (1962).
W. Zawadski, J. Kolodziejczak, Phys. Stat. Sol., 6, 409, 419 (1964).
44. R. Barrie, Proc. Phys. Soc. Lond., 69B, 553 (1956).
45. A.I. Anselm, Einführung in die Halbleitertheorie, Akademie-Verlag, Berlin (1964).
46. J.M. Radcliffe, Proc. Phys. Soc. Lond., B69, 675 (1955).
47. L.L. Korenblit, D. Mashovets, S.S. Shalyt, Sov. Phys. - Solid State, 6, 438 (1964).
S.A. Aliev, L.L. Korenblit, S.S. Shalyt, Sov. Phys. - Solid State, 8, 565 (1966).
48. L.L. Korenblit, V.E. Sherstobitov, Sov. Phys. - Semicond., 2, 573 (1968).
49. S.A. Aliev, et al., Proc. Int. Conf. Phys. of Semicond., Moscow, 659, (1968).
50. D. Armitage, H.J. Goldsmid, J. Phys. C (Solid State Phys.), 2, 2138, 2389 (1969).
51. J.M. Ziman, Electrons and Phonons, Oxford Clarence Press, (1960).

52. D.J. Howarth, E.H. Sondheimer, Proc. Roy. Soc., A219, 53 (1956).
53. T.C. Harman, J. Phys. Chem. Sol., 25, 931 (1964).
54. W. Szymanska, Phys. Stat. Sol., 23, 69 (1967).
R.R. Galazka, L. Sosnowski, Phys. Stat. Sol., 20, 113 (1967).
55. S.H. Groves, R.N. Brown, C.R. Pidgeon, Phys. Rev., 161, 779 (1967).
56. H. Ehrenreich, Phys. Rev., 120, 1951 (1960); J. Appl. Phys., 32, 2155 (1961).
57. D.G. Thomas (ed.), II-VI Semiconducting Compounds, International Conference, Benjamin (New York), p. 982,(1967).
58. N.A. Goryunova, The Chemistry of Diamond-like Semiconductors, Chapman and Hall (London), (1965).
59. S.S. Shalyt, S.A. Aliev, Sov. Phys. - Solid State, 6, 1563 (1965).
60. H. Ehrenreich, J. Phys. Chem. Sol., 2, 131 (1957).
61. P.W. Sparks, C.A. Swenson, Phys. Rev., 163, 779 (1967).
62. T.C. Cetas, C.R. Tilford, C.A. Swenson, Phys. Rev., 174, 835 (1968).
63. F. Kelemen, E. Cruceanu, D. Niculescu, Phys. Stat. Sol., 11, 865 (1965).
64. L. Giraudier, J. Phys., 26, 129A (1965).
65. J. Schröder, Rev. Sci. Instr. 34, 615 (1963).
66. F.A.P. Blom, intern rapport THE (1968). (In Dutch).
67. R.A. Smith, Semiconductors, University Press, Cambridge (1959).
68. Ya. Agaev, O. Mosanov, O. Ismailov, Sov. Phys.-Semicond., 1, 978 (1968).
69. R.K. Willardson, A.C. Beer (ed.), Semiconductors and Semimetals, Vol.1, Academic Press (New York), (1966).

LIST OF SYMBOLS

B	magnetic induction
e	absolute value of the electron charge
E	electron energy relative to an external reference level
E_B	band edge energy relative to an external reference level
E_g	band gap between valence and conduction band
$f; f_o$	distribution function; Fermi-Dirac distribution function
f_H, f_R	correction factors due to finite dimensions of a specimen
F	force function
g	symbol for a general function
G_j	transport integral
$h; \hbar$	Planck's constant; $h/2\pi$
$I_i; J_j$	transport integrals
J	electric current density
k	wave number
k_o	Boltzmann's constant
K_i	transport integral
l	length of a specimen
L	transport integral
L, L_o	experimental and theoretical Lorenz numbers
m^*	electron effective mass
m_o	free electron mass
$m^*(0)$	effective mass at the bottom of a Kane conduction band
$m_\perp^*, m_\parallel^*$	effective masses with magnetic field perpendicular and parallel to the c-axis of a crystal
n	electron concentration
N^i, N^a	isothermal and adiabatic transverse Nernst coefficients
P	matrix element of Kane's theory
Q	quantity related to P
r	scattering parameter
r	position coordinate
R_H^i	isothermal Hall coefficient
S	Righi-Leduc coefficient
T	absolute temperature

u	unaveraged mobility
u_{ε_F}	mobility at the Fermi level
v	group velocity
W	heat current density
x	reduced kinetic energy of an electron
x_g	reduced band gap
x,y,z	position coordinates

α^i, α^a	isothermal and adiabatic Seebeck coefficients
β	collection of parameters and constant, proportional to magnetic induction
γ	non-parabolicity parameter
$\nabla(\nabla_x, \nabla_y, \nabla_z)$	gradient vector
Δ	difference symbol
Δ_{so}	spin-orbit splitting of the valence band
ε	kinetic energy relative to conduction band edge
ε_F	Fermi level relative to conduction band edge
ζ	Fermi level relative to an external reference level
η	reduced Fermi level
Θ, Θ_o	Debije temperatures at arbitrary temperature and at absolute zero
Θ_L	Debije temperature for longitudinal optical phonons
κ^i, κ^a	isothermal and adiabatic thermal conductivities
κ_E, κ_L	electronic and lattice components of K
μ, μ_H, μ_T	conductivity mobility, Hall mobility, thermal mobility
ρ^i	isothermal resistivity
σ^i	isothermal conductivity
τ	relaxation time
Ψ	function of ω, τ and F
ω	cyclotron frequency

SUMMARY

Measurements of the thermomagnetic transport phenomena, in addition to those of the galvanomagnetic effects, can give valuable information on the band structure and the nature of the scattering of the charge carriers in semiconductors. In this thesis measurements are described and analysed concerning the thermomagnetic effects in the semiconducting compound cadmium arsenide Cd_3As_2.

In Chapter 1 a short review is given of the physico-chemical properties, and the electrical and thermal transport phenomena in this II-V-compound, reported in the literature. The existence of a solid-solid transformation at about 140°C below the melting point, which causes a considerable change in the volume of the unit cell, is mainly responsible for the difficulty of preparing crackfree samples with suitable dimensions. There is a striking similarity between the electrical transport properties of this compound and those of InSb, HgTe and HgSe, such as high electron mobility and a narrow energy band gap.

Chapter 2 deals with the experimental methods which are used for the preparation of the samples and for the measurements of the thermomagnetic effects. By using a quenching method, it appears possible to obtain relatively large, crackfree polycrystalline samples. The chapter concludes with corrections and conversions which are necessary owing to the finite length-to-width ratios of the samples and the differences between the adiabatic and isothermal transport coefficients.

Chapter 3 gives a review of the theory of the thermomagnetic effects in strongly degenerate n-type semiconductor with a non-parabolic conduction band.

In Chapter 4 the experimental results are given and discussed. By using an extrapolation method, the saturation values of the Seebeck coefficients are determined from the measurements of the changes of these coefficients in a magnetic field. From these saturation values and the electron concentrations the electron effective masses are calculated. This method of determining m^* does not require the knowledge of the scattering mechanism. The electron effective mass increases from about 0.032 m_o to 0.075 m_o with increasing electron concentration from about 0.7 to

13×10^{24} m^{-3}. The dependence of the effective mass on concentration has been explained by a non-parabolic conduction band, as proposed for InSb by Kane. The room temperature values of the parameters of Kane's model applied to Cd_3As_2 are found to be $P = 8.1 \times 10^{-8}$ eVcm, $E_g = 0.15$ eV and $m^*(0) = 0.012\ m_o$.

Applying the theory of Kolodziejczak et al., the scattering parameter has been determined from the ratio between the saturation and zero-field values of the Seebeck coefficient. This analysis leads to the conclusion that within the investigated range of electron concentrations the scattering is caused by interactions with optical lattice vibrations. Numerical calculations with the theory of Harman and Honig have been carried out for the theoretically expected dependences of the various transport coefficients on magnetic induction. Comparisons between the experimental and theoretical magnetic field dependences clearly show that the transport effects at room temperature can be described very well by the above mentioned band model and scattering mechanism. A confirmation of these conclusions has also been given by the concentration dependence of the zero-field Seebeck coefficient. The experimental results at liquid nitrogen temperature cannot be explained by the assumption of only one type of scattering, which, among other causes, is probably due to the imperfection of our samples.

Since the electronic part of the total thermal conductivity in Cd_3As_2 has the same order of magnitude as the lattice part, these contributions can be separated by measuring the change of the thermal conductivity in a magnetic field. If the electronic thermal conductivity is known, the Lorenz number can be obtained. The experimental Lorenz numbers in some of our samples are smaller than the theoretical ones, which indicates a partially inelastic scattering of the electrons. The presence of this partially inelastic scattering mechanism is also confirmed by the fact that the thermal mobilities are smaller than the Hall mobility. The measurements have been analysed in terms of the theory of Korenblit and Sherstobitov for partially inelastic collisions between conduction electrons and optical phonons at temperatures near the Debije temperature.

S A M E N V A T T I N G

Metingen van de thermomagnetische transportverschijnselen kunnen, naast die van de galvanomagnetische effekten, waardevolle informatie geven over de bandenstruktuur en de aard van de verstrooiing van de ladingsdragers in halfgeleiders. In dit proefschrift worden metingen van de thermomagnetische effekten aan de halfgeleidende verbinding cadmium arsenide, Cd_3As_2, beschreven en geanalyseerd.

In hoofdstuk 1 wordt een kort overzicht gegeven van de literatuur over de physisch-chemische eigenschappen, en de elektrische en thermische transportverschijnselen in deze II-V-verbinding. Vanwege het optreden van een vast-vast overgang bij ongeveer 140°C beneden het smeltpunt, waarmee een aanzienlijke verandering van de afmetingen van de elementaire cel gepaard gaat, is het moeilijk om scheurvrije preparaten met geschikte afmetingen te vervaardigen. Wat de elektrische transport eigenschappen betreft, is er een opvallende gelijkenis met de verbindingen InSb, HgTe en HgSe, zoals de hoge beweeglijkheid van de elektronen en de kleine bandafstand.

In hoofdstuk 2 worden de experimentele technieken besproken die gebruikt zijn ter vervaardiging van de preparaten en meting van de thermomagnetische effekten hieraan. Bij de bereiding wordt een afschrikmethode toegepast, waarmee het mogelijk blijkt om relatief grote, scheurvrije polykristallijne staafjes te verkrijgen. Verder wordt er aandacht geschonken aan de korrekties en omrekeningen die dienen te worden uitgevoerd, ten gevolge van de eindige lengte-breedte verhouding van de preparaten en het verschil tussen de adiabatische en isotherme transportkoëfficiënten.

Hoofdstuk 3 bevat een overzicht van de theorie over de thermomagnetische effekten in sterk gedegenereerde n-type halfgeleiders met een niet-parabolische geleidingsband.

De experimentele resultaten worden gegeven en besproken in hoofdstuk 4. Uit de metingen van de veranderingen van de Seebeck koëfficiënten in een magnetisch veld worden de verzadigingswaarden van deze koëfficiënten door extrapolatie bepaald. Samen met de elektronenkoncentraties worden hieruit de effektieve massa's van de geleidingselektronen berekend. Deze methode ter bepaling van de effektieve

massa vereist niet de kennis van het verstrooiïngsmechanisme. Met toenemende elektronenkoncentratie van ongeveer 0.7 tot 13 × 10^{24} m^{-3} neemt de effektieve massa toe van ongeveer 0.032 m_o tot 0.075 m_o. Dit verloop van de effektieve massa met het aantal vrije elektronen kan goed worden verklaard met een niet-parabolische geleidingsband, zoals Kane heeft voorgesteld voor InSb. De waarden die gevonden worden voor de karakteristieke parameters van dit bandenmodel, bedragen voor Cd_3As_2 bij kamertemperatuur: P = 8.1 × 10^{-8} eVcm, E_g = 0.15 eV en $m^*(0)$ = 0.012 m_o.

Uit de verhouding tussen de verzadigingswaarde en de waarde van de Seebeck koëfficiënt buiten het magnetisch veld, is de verstrooiïngsparameter bepaald, onder gebruikmaking van de theorie van Kolodziejczak e.a. Dit leidt tot de conclusie dat, in het door ons onderzochte gebied van elektronenkoncentraties, de vertrooiïng bij kamertemperatuur moet worden toegeschreven aan interakties met optische roostertrillingen. Aan de hand van de theorie van Harman en Honig zijn numerieke berekeningen uitgevoerd voor het theoretische verloop van de diverse transport koëfficiënten als funktie van de magnetische inductie. De vergelijkingen van de experimenteel gevonden met de theoretisch berekende afhankelijkheden tonen duidelijk aan dat het transportmechanisme in Cd_3As_2 bij kamertemperatuur goed beschreven kan worden met het bovengenoemde verstrooiïngs- en bandenmodel. Ook het verband tussen de Seebeck koëfficiënt en de elektronenconcentratie bevestigt deze konklusie. Bij vloeibare stikstoftemperatuur zijn de meetresultaten niet met één verstrooiingsmechanisme te verklaren, hetgeen waarschijnlijk o.a. te wijten is aan onzuiverheden in onze preparaten.

Daar in Cd_3As_2 het elektronenaandeel in de totale warmtegeleidbaarheid van dezelfde orde-grootte is als het roosteraandeel, is het mogelijk deze bijdragen van elkaar te scheiden door meting van de verandering van de warmtegeleidbaarheid in een magnetisch veld. Deze scheiding maakt het mogelijk het Lorenz getal te bepalen. In enkele preparaten is dit kleiner dan het theoretische Lorenz getal, hetgeen duidt op een gedeeltelijke inelastische verstrooiïng van de elektronen. Het optreden van een gedeeltelijk inelastisch verstrooiïngsmechanisme wordt ook bevestigd door het verschil dat gevonden wordt tussen de Hall beweeglijkheid en de thermische beweeglijkheid. Bij de analyse is gebruik gemaakt van de theorie van Korenblit en Sherstobitov over gedeeltelijk inelastische botsingen tussen elektronen en optische fononen bij temperaturen in de buurt van de Debije temperatuur.

D A N K W O O R D

Op de eerste plaats wil ik gaarne mijn ouders bedanken voor de gelegenheid die zij mij hebben geboden om te studeren. Daarnaast zou ik dit proefschrift nooit hebben kunnen voltooien zonder de onuitsprekelijk vele steun die ik van mijn vrouw gehad heb, vooral in de laatste fase van het werk.

Mijn dank gaat verder uit naar Prof.dr.F. van der Maesen voor de vele vruchtbare discussies die ik met hem heb mogen voeren, vooral met betrekking tot de theoretische achtergronden van de transportverschijnselen in de vaste stof. De heren A. Huyser, A.B.D. v.d. Meer, J.Th. Schrama en A.J. v.d. Steld die als afstudeerders een bijdrage aan het onderzoek geleverd hebben, verdienen eveneens mijn dank; vooral de heer v.d. Meer wil ik speciaal mijn erkentelijkheid betuigen voor het chemisch-preparatieve werk dat hij deed. Voor de hulp bij de technische problemen en de uitvoering van een aantal zeer tijdrovende metingen, betuig ik gaarne mijn dank aan de heer P.A.M. Nouwens.

Tenslotte gaat mijn dank uit naar degenen die hebben meegewerkt aan de uiteindelijke uitvoering van deze dissertatie: mej.A. Latour voor het typen van het manuscript, mej.M. Gruyters voor het verzorgen van het tekenwerk en de heer H.J.A. van Beckum voor de correctie van de Engelse tekst.

L E V E N S B E R I C H T

Op verzoek van de Senaat der Technische Hogeschool volgen hier enkele persoonlijke gegevens.

De schrijver van dit proefschrift werd geboren op 20 juli 1939 te Haps (N.B.) en volgde aldaar lager onderwijs. Na het eindexamen HBS-B te hebben afgelegd aan het Chrysostomus college te Boxmeer in 1957, begon hij zijn studie aan de Technische Hogeschool Eindhoven in de afdeling der

Elektrotechniek. In 1960 veranderde hij van studierichting en zette zijn studie voort aan de inmiddels opgerichte onderafdeling der Technische Natuurkunde. Het examen voor natuurkundig ingenieur werd afgelegd in 1964, met als afstudeerwerk een onderzoek aan éénkristallijn bariumtitanaat. Sinds 1964 is hij in dienst van deze hogeschool als wetenschappelijk medewerker in de groep materiaalkunde, waar hij vanaf 1966 gewerkt heeft aan het onderwerp van deze dissertatie.

STELLINGEN

Behorende bij het proefschrift van F.A.P. Blom

11 december 1970

STELLINGEN

I

De bewering van Long, dat uit metingen van de transportverschijnselen in halfgeleiders waarden van de thermische bandafstand bepaald kunnen worden, is aanvechtbaar wanneer het thermomagnetische effekten betreft.

D. Long, Energy Bands in Semiconductors, Interscience Publishers, New York, 70 (1968).

II

De toepassing van Zener-diodes in warmtegeleidbaarheidsmetingen van vaste stoffen via de absolute methode, biedt voordelen boven het gebruik van een elektrische weerstand als warmtebron.

Dit proefschrift, section 2.2.

III

De veronderstelling van Ballentyne en Lovett dat de effektieve elektronenmassa in Cd_3As_2 sterk zou toenemen bij lage temperaturen wordt door hun experimenten onvoldoende gesteund en wekt de indruk in hoofdzaak te berusten op een onjuiste interpretatie van de metingen van Haidemenakis e.a.

D.W.G. Ballentyne, D.R. Lovett, Brit. J. Appl. Phys., 1, 585 (1968).
E.D. Haidemenakis, e.a., Solid State Comm., 4, 65 (1966).

IV

Het verdient aanbeveling om het fasediagram van het binaire stelsel Cd-As opnieuw te onderzoeken.

M. Hansen, Constitution of Binary Alloys, McGraw-Hill, New York, 156 (1958).

V

De wijze waarop Tsidilkovskii de omrekeningen van adiabatische naar isotherme transportkoëfficiënten uitvoert is omslachtig en kan aanleiding geven tot misverstanden.

I.M. Tsidilkovskii, Thermomagnetic Effects in Semiconductors, Infosearch, London, 181 (1962).

VI

Het heeft voordelen om bij de theoretische beschrijving van thermoelektrische energieomzetters de koppelfaktor k^2 in te voeren in plaats van de "figure of merit" ZT.

C. Zwikker, Fysische Materiaalkunde, Wetenschappelijke Uitgeverij, Amsterdam, deel 1, 158 (1966).

VII

Bij de verklaring van de stroomoscillaties in GaSe hebben Levialdi en Romeo de invloed van de kontakten ten onrechte buiten beschouwing gelaten.

A. Levialdi, N. Romeo, Nuovo Cimento, 63B, 41 (1969).

VIII

De door Kaidanov en Chernik gebruikte methode voor het meten van het transversale Nernst effekt is aan bedenkingen onderhevig.

V.I. Kaidanov, I.A. Chernik, Sov. Phys.-Semicond., 1, 1159 (1967).

IX

De argumenten, welke door Ghare e.a. aangevoerd worden ter verklaring van de elektrische geleidbaarheidsmetingen aan $CuMn_2O_4$ zijn aanvechtbaar.

D.B. Ghare, A.P.B. Sinha, L. Singh, J. Material Science, 3, 389 (1968).

X

In leerboeken over halfgeleiders wordt in het algemeen te weinig aandacht geschonken aan het verschil tussen de relatieve en de absolute thermokracht.

XI

Volleybal, gespeeld door veteranen, zou voor de toeschouwers in belangrijke mate aan aantrekkelijkheid kunnen winnen indien de nethoogte aan de spelersleeftijd wordt aangepast.